The Company of Biologists

RESEARCH ARTICLE

Neurodegenerative disease-associated protein aggregates are poor inducers of the heat shock response in neuronal cells

Rebecca San Gil[1,2,3], Dezerae Cox[4], Luke McAlary[1,2], Tracey Berg[1,2], Adam K. Walker[3], Justin J. Yerbury[1,2], Lezanne Ooi[1,2] and Heath Ecroyd[1,2,*]

ABSTRACT

Protein aggregates that result in inclusion formation are a pathological hallmark common to many neurodegenerative diseases, including amyotrophic lateral sclerosis, Parkinson's disease and Huntington's disease. Under conditions of cellular stress, activation of the heat shock response (HSR) results in an increase in the levels of molecular chaperones and is a first line of cellular defence against inclusion formation. It remains to be established whether neurodegenerative disease-associated proteins and inclusions are themselves capable of inducing an HSR in neuronal cells. To address this, we generated a neuroblastoma cell line that expresses a fluorescent reporter protein under conditions of heat shock transcription factor 1 (HSF1)-mediated HSR induction. We show that the HSR is not induced by exogenous treatment with aggregated forms of recombinant α-synuclein or the G93A mutant of superoxide dismutase-1 ($SOD1^{G93A}$) nor intracellular expression of $SOD1^{G93A}$ or a pathogenic form of polyglutamine-expanded huntingtin (Htt^{72Q}). These results suggest that pathogenic proteins evade detection or impair induction of the HSR in neuronal cells. A failure of protein aggregation to induce an HSR might contribute to the development of inclusion pathology in neurodegenerative diseases.

This article has an associated First Person interview with the first author of the paper.

KEY WORDS: HSF1, Heat shock response, Inclusions, Neurodegenerative disorders, Protein aggregation

INTRODUCTION

The formation of intracellular protein inclusions is a characteristic hallmark of neurodegenerative diseases, such as amyotrophic lateral sclerosis (ALS), Parkinson's disease and Huntington's disease (Chiti and Dobson, 2017). In these diseases, intrinsically disordered or partially unfolded proteins self-associate through hydrophobic interactions between regions that are usually buried in the native conformation (Hipp et al., 2019). Interactions between misfolded

[1]Illawarra Health and Medical Research Institute, Wollongong, NSW 2522, Australia. [2]Molecular Horizons and School of Chemistry and Molecular Bioscience, University of Wollongong, Wollongong, NSW, Australia. [3]Neurodegeneration Pathobiology Laboratory, Queensland Brain Institute, University of Queensland, St Lucia, QLD 4072, Australia. [4]Department of Biochemistry and Molecular Biology, Bio21 Molecular Science and Biotechnology Institute, University of Melbourne, Parkville, VIC 3052, Australia.

*Author for correspondence (heathe@uow.edu.au)

R.S.G., 0000-0001-5725-5512; D.C., 0000-0002-5345-8360; L.M., 0000-0002-1764-3809; A.K.W., 0000-0001-7954-5801; J.J.Y., 0000-0003-2528-7039; L.O., 0000-0001-9241-8268; H.E., 0000-0001-7574-0044

monomers can nucleate the formation of toxic protein oligomers that are the precursors of inclusions (Kopito, 2000). Inclusions can be diverse with regards to their size, localisation, and composition. Specific inclusion subtypes have been identified, including those known as IPOD (Insoluble Protein Deposit), JUNQ (Juxtanuclear Quality Control Compartment) and RISCI (RNA Interactor Specific Compartments/Inclusions) (Farrawell et al., 2015; Kaganovich et al., 2008; Kayatekin et al., 2014; Polling et al., 2014; Matsumoto et al., 2006; Whiten et al., 2016). The roles of different inclusion types may include interacting with proteostasis pathways and acting as terminal storage sites for destabilised proteins (Kayatekin et al., 2014; Polling et al., 2014; Matsumoto et al., 2006; Farrawell et al., 2015). There is increasing evidence to suggest that the misfolding of monomers and subsequent formation of oligomeric intermediates are the processes responsible for generating toxic species that trigger cellular stress and neurotoxicity: inclusion formation might actually represent a neuroprotective process (Winner et al., 2011; Leitman et al., 2013; Zhu et al., 2018; Bolognesi et al., 2010).

The process of protein aggregation has been strongly correlated with the death of neurons in neurodegenerative diseases (Brettschneider et al., 2013, 2014; Braak et al., 2006, 2003). The progression of inclusion pathology, from a focal site of onset to other regions of the central nervous system (CNS), may be driven by the movement of aggregated proteins in the extracellular space (Vaquer-Alicea and Diamond, 2019). Therefore, aggregation is seeded in neighbouring cells (including neurons) via prion-like propagation (Victoria and Zurzolo, 2017; Jucker and Walker, 2013; Zeineddine and Yerbury, 2015; Hanspal et al., 2017; McAlary et al., 2019; Peng et al., 2020). This spread of disease pathology throughout the CNS suggests a widespread inability of cells to prevent the initial events leading to protein aggregation and the propagative seeding events that follow.

Cells have several mechanisms of defense against disturbances in proteostasis (Yerbury et al., 2016). These mechanisms usually function to ensure the correct folding, function and turnover of proteins in the cell, and prevent the negative effects of proteostasis imbalance on cell viability. The heat shock response (HSR) is one such mechanism of proteostasis and acts as a first line of defense against protein destabilisation, misfolding and aggregation (San Gil et al., 2017b). Under conditions of cellular stress, an increasing intracellular abundance of destabilised proteins can lead to the activation of heat shock transcription factor 1 (HSF1). HSF1 translocates into the nucleus and binds heat shock elements (HSEs; a pentameric sequence nGAAn, where 'n' represents any nucleotide) in the promoter elements of HSF1-target genes (Pelham, 1982; Sorger et al., 1987; Amin et al., 1988; Xiao and Lis, 1988). Induction of the HSR results in rapid and dramatic upregulation of a subset of the heat shock protein (Hsp) family of molecular chaperones. Molecular chaperones are capable of stabilising and re-folding misfolded proteins, as well as trafficking

damaged proteins to the proteasomal or autophagy-lysosomal pathways for degradation (Leak, 2014). There is a wealth of evidence in cell-based and *in vivo* models demonstrating that the overexpression of individual Hsps significantly ameliorates neurodegenerative disease-associated protein aggregation (San Gil et al., 2017b; Webster et al., 2019; Kakkar et al., 2014). For example, overexpression of HSPB1 (Hsp27) or HSPB5 (αB-crystallin, also known as CRYAB) results in a 30–40% decrease in Neuro-2a cells with α-synuclein inclusions (Cox and Ecroyd, 2017). Moreover, overexpression of HSF1 itself can prevent protein aggregation, presumably via its capacity to increase the expression of molecular chaperones. For example, in a mutant superoxide dismutase-1 (SOD1) mouse model of ALS, overexpression of HSF1 leads to a 34% decrease in the level of insoluble SOD1$^{H46R/H48Q}$ in spinal cord tissue compared to controls (Lin et al., 2013). The overexpression of constitutively active HSF1 in the R6/2 mouse model of Huntington's disease leads to a 21% decrease in the proportion of nuclei with inclusions and extended survival (mean survival 122 d in R6/2-HSF1Tg compared to 107 d in R6/2 mice) (Fujimoto et al., 2005). Whilst the activation of HSF1 or increased expression of Hsps can ameliorate protein aggregation and extend survival in models of neurodegenerative disease, it remains to be definitively established whether aggregation-prone proteins or the inclusions they form are themselves capable of inducing an endogenous HSF1-mediated HSR.

At the whole tissue level, there is evidence to suggest that Hsp expression is altered with neurodegenerative disease progression [for a comprehensive review see San Gil et al. (2017b)]. For example, recent work that involved studying human postmortem ALS spinal cord and motor cortex tissue demonstrated that *HSPA5, DNAJB1* and *HSPB1* mRNA are upregulated and *DNAJA1* and *HSPA8* are downregulated compared to healthy controls (Montibeller et al., 2020; Montibeller and de Belleroche, 2018). With regards to cells of the CNS, the prevailing hypothesis is that neurons have a high-threshold for HSR induction relative to other cell types, such as astroglia (San Gil et al., 2017b; Chen et al., 2016; Mimoto et al., 2012; Wang et al., 2008; Hay et al., 2004; Batulan et al., 2003). However, it is currently not known whether aggregation-prone proteins, or indeed the inclusions themselves, are capable of inducing an HSF1-mediated HSR in HSR-competent cells. To evaluate this, we generated a stable cell line derived from mouse neuroblastoma Neuro-2a cells that expresses a fluorescent reporter under the control of a truncated *HSPA1A* promoter comprised of eight putative HSEs. We then used this stable cell line to quantitatively assess the kinetics and magnitude of HSR induction after exogenous application of protein aggregates and throughout intracellular inclusion formation. Moreover, using these cells, we dissected the effects of protein pathogenicity (defined here as proteins or mutant proteins whose aggregation is associated with human disease), inclusion size, intracellular protein concentration and rate of inclusion formation on HSR induction.

We report that the exogenous application (SOD1^{G93A} or α-synuclein) or intracellular expression (SOD1^{G93A} or polyglutamine-expanded huntingtin, Htt^{72Q}) of pathogenic proteins failed to induce an HSR in cells. In contrast, the intracellular aggregation of a non-pathogenic protein – a destabilised version of firefly luciferase (Fluc) (Gupta et al., 2011) – did result in HSR induction in a significant proportion of cells. In addition, our work demonstrates that the intracellular levels of the aggregation-prone proteins tested is the most significant determinant of HSR induction such that there is a positive correlation between the concentration of the aggregation-prone protein and the proportion of cells with an

activated HSR. The relatively poor induction of the HSR by pathogenic proteins compared to non-pathogenic Fluc could explain, at least in part, the ability of disease-related inclusions to evade proteostasis pathways.

RESULTS
Generation and validation of an HSR reporter cell line
To investigate the activation of the HSR, stable Neuro-2a cell lines were generated in which expression of a fluorescent protein (EGFP) was used to report on HSR induction. These cells also constitutively express mCherry to account for changes in cell number or transcription rates over time with different treatment paradigms. To validate that this stable cell line reports on HSR induction, the cells were first treated with known inducers of the HSR, namely CdCl$_2$, heat shock, and celastrol (a compound identified in a drug screen as a potent inducer of the HSR) (Westerheide et al., 2004; Heemskerk et al., 2002). The fluorescent reporter, EGFP, has a half-life of ∼27 h (Corish and Tyler-Smith, 1999), therefore these experiments were performed over a timeframe that would facilitate the accumulation of EGFP after HSR induction in order to assess the magnitude of the HSR. Concentration-response experiments were conducted to determine the concentration of CdCl$_2$ (0–33 μM) and celastrol (0–1 μM) that induces a maximal HSR (Fig. S2). Based on these results, subsequent experiments used 10 μM CdCl$_2$ and 0.75 μM celastrol over a 24 h timeframe, which were the lowest concentrations that induced a maximal HSR in Neuro-2a (HSE: EGFP) cells.

By tracking the mCherry fluorescence intensity over time, changes in cell number (i.e. cell growth or death) was able to be determined with each treatment (Fig. 1A,B). Heat shock was non-lethal and cell growth proceeded similarly to the no treatment sample, such that there was a twofold increase in mCherry fluorescence intensity over 24 h. CdCl$_2$ treatment stopped cell division, and celastrol treatment resulted in a decline in mCherry fluorescence intensity over the 24 h timecourse, consistent with it being toxic to the cells (Fig. 1B). Following treatment with 10 μM CdCl$_2$, heat shock (42°C for 2 h), or 0.75 μM celastrol, there was a time-dependent increase in EGFP fluorescence intensity in Neuro-2a (HSE:EGFP) cells (Fig. 1A,C). Fluorescence was first detected 2–4 h following heat shock treatment of Neuro-2a (HSE:EGFP) cells and reached a maximal response after 12 h (Fig. 1C). Immunoblot analysis of heat shocked parental Neuro-2a cells showed that HSF1 was hyper-phosphorylated for up to 2 h post-heat shock (Fig. S3). Phosphorylation of HSF1 was followed by a time-dependent increase in Hsp70 (a well characterised target of HSF1 activation) such that it was first detectable 15 min after heat shock and reached a maximum after 6–12 h (Fig. S3). The earlier detection of Hsp70 by immunoblotting following heat shock of the parental Neuro-2a cells compared to detection of EGFP by live-cell imaging following heat shock of Neuro-2a (HSE:EGFP) cells is likely attributable to the increased sensitivity of immunoblotting. In any case, these data demonstrate that the Neuro-2a (HSE:EGFP) reporter cell line enables live-cell imaging to follow the dynamics of the HSR in single cells in real time.

The time taken to induce the HSR and to reach maximum EGFP fluorescence varied between treatment types. The expression of EGFP was induced significantly faster after heat shock (mean± s.e.m. of 5.1±0.2 h) compared to treatment with CdCl$_2$ or celastrol (mean±s.e.m. of 11±0.6 h and 8.3±1.5 h, respectively; Fig. 1D) [one-way ANOVA, $F_{(2, 6)}=28.28$, $P=0.0009$] as measured by the time taken to reach half maximal EGFP fluorescence. Treatment with each of these classical inducers of the HSR resulted in a
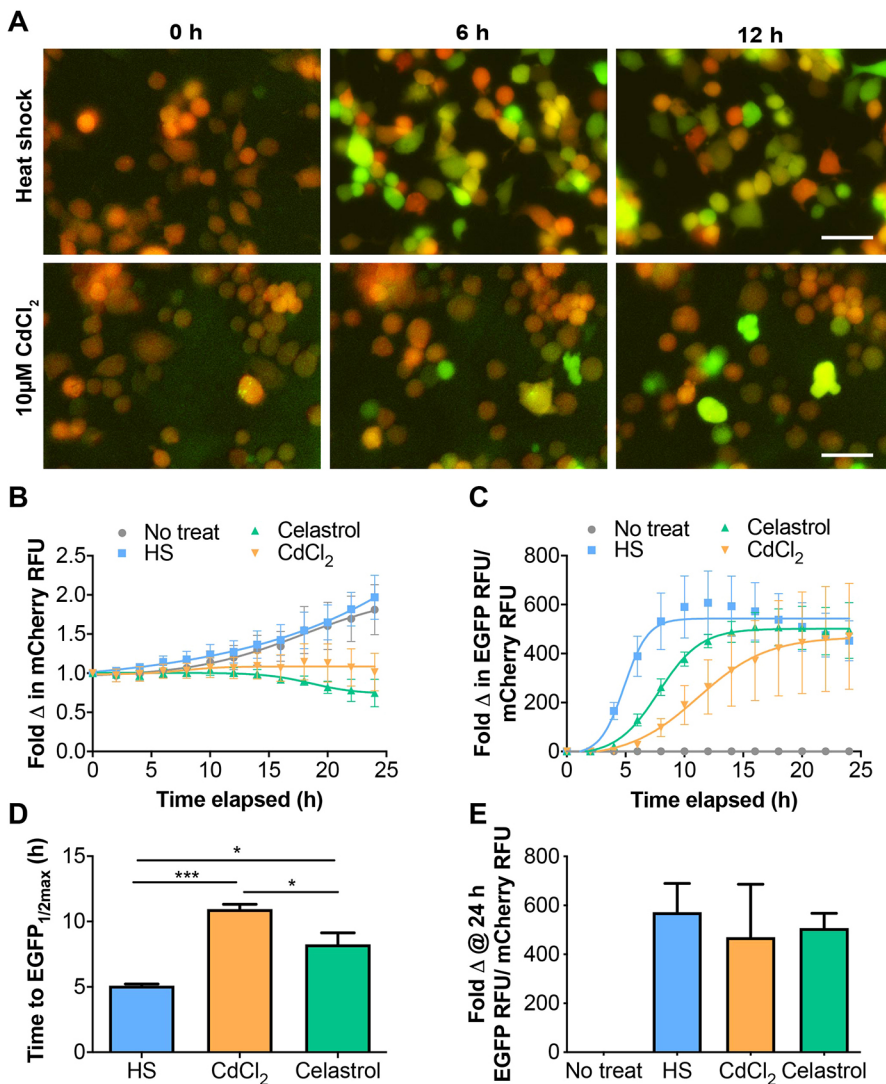
Fig. 1. Neuro-2a (HSE:EGFP) cells enable time-resolved, specific and sensitive quantification of HSR induction. (A) Neuro-2a (HSE:EGFP) cells stably expressing mCherry were treated with 10 μM CdCl₂, 0.75 μM celastrol or heat shocked (42°C for 2 h) and imaged every 2 h to monitor EGFP expression. Representative overlay images of mCherry and EGFP fluorescence are shown after 0, 6 and 12 h of treatment. Scale bars: 50 μm. (B) The fold change in mCherry fluorescence intensity over time. (C) The fold change in EGFP fluorescence intensity over time normalised to mCherry fluorescence intensity to account for changes in cell density during the experiment. (D) The kinetics of HSR induction as determined by the time taken to reach half maximal EGFP fluorescence. (E) The magnitude of HSR induction as determined by EGFP fluorescence after 24 h of treatment with each stress. Data shown are the mean±s.e.m. of three independent repeats. Differences between the means were assessed using a one-way ANOVA followed by Tukey's post hoc test. *$P<0.05$, ***$P<0.001$.

significant increase in the magnitude of EGFP expression in Neuro-2a (HSE:EGFP) cells compared to no treatment [one-way ANOVA, F (3,8)=4.265, P=0.0448] (Fig. 1E). However, there were no differences observed between the magnitude of HSR induction and treatment type in Neuro-2a (HSE:EGFP) cells as determined by the fold change in EGFP fluorescence intensity at 24 h (Fig. 1E). Therefore, the Neuro-2a (HSE:EGFP) reporter cell line developed in this study is a sensitive and accurate tool that can be used to track the kinetics and magnitude of HSR induction in live neuronal-like cells.

Extracellular protein aggregates do not induce an HSR

There is increasing evidence that disease-associated protein aggregation propagates through the CNS from the site of onset in a prion-like mechanism. This process likely involves the release of misfolded and aggregated protein from neurons into the extracellular space and their subsequent uptake by surrounding cells (Jucker and Walker, 2013; Zeineddine et al., 2015; Zeineddine and Yerbury, 2015). We therefore sought to determine whether cells respond to extracellular aggregated protein by inducing an HSR. To test this, recombinant human α-synuclein and SOD1^G93A were aggregated in vitro. There was a significant increase in Thioflavin T (ThT) fluorescence of the aggregated α-synuclein sample compared to monomeric α-synuclein and buffer alone, indicative of an

increase in β-sheet structure with aggregation (Fig. 2A). Transmission electron microscopy (TEM) indicated that the α-synuclein had formed long, mature fibrils greater than 2 μm in length (Fig. 2A, inset). The formation of SOD1^G93A aggregates was monitored by an in situ ThT binding assay; there was a time-dependent increase in ThT fluorescence relative to buffer alone (Fig. 2B). The SOD1^G93A aggregates formed in these assays had an irregular amorphous structure and were less than 80 nm in length (Fig. 2B, inset). Taken together, the ThT and TEM data indicate that the SOD1^G93A aggregates formed in this study contain an underlying β-sheet structure, but did not assemble into highly-ordered fibrils.

Non-aggregated and aggregated forms of α-synuclein and SOD1^G93A were applied to Neuro-2a (HSE:EGFP) cells and the cells were monitored for HSR induction by time-lapse live-cell imaging (Fig. 2C,D). There was no significant difference in EGFP fluorescence in cells treated for 20 h with either 1 μM or 10 μM of non-aggregated or aggregated α-synuclein or SOD1^G93A (Fig. 2E,F), and this remained the case even up to 72 h after treatment (data not shown). In contrast, the positive control CdCl₂ treatment induced an HSR in these cells (Fig. 2E,F). Thus, when applied extracellularly to Neuro-2a (HSE:EGFP) cells, neither α-synuclein fibrils nor SOD1^G93A aggregates induced an HSR.
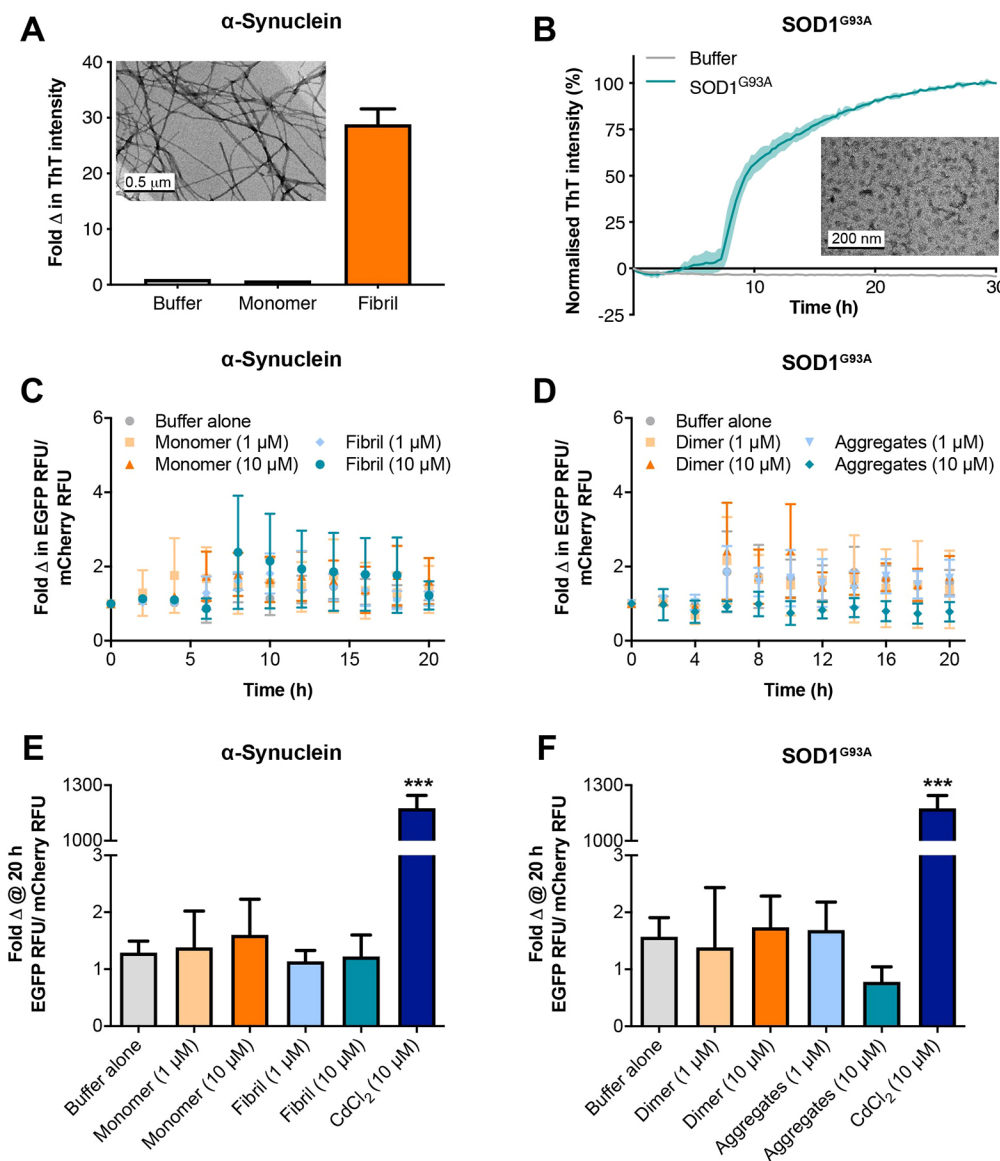
Fig. 2. Disease-associated protein aggregates do not induce an HSR in Neuro-2a (HSE:EGFP) cells when applied extracellularly. The formation of (A) α-synuclein fibrils, and (B) SOD1^{G93A} aggregates was confirmed by ThT fluorescence and TEM (insets). Scale bars: 0.5 µm and 200 nm, respectively. Data shown are the mean±s.e.m. of two technical replicates. (C,D) Monitoring induction of the HSR using live-cell imaging. Time course of EGFP RFU normalised to mCherry RFU of Neuro-2a (HSE: EGFP) cells treated with (C) monomeric or fibrillar α-synuclein, or (D) dimeric or aggregated SOD1^{G93A}. (E,F) The magnitude of HSR activation as determined by the EGFP RFU/mCherry RFU 20 h after application of the protein aggregates or CdCl$_2$. Data shown are the mean±s.e.m. of at least three independent repeats. Differences between the means were assessed using a one-way ANOVA followed by Dunnet's post hoc test (comparing to buffer alone control). ***P<0.001.

Intracellular expression and aggregation of pathogenic proteins is a poor inducer of the HSR

We next used the Neuro-2a (HSE:EGFP) cells to investigate whether the aggregation of proteins into inclusions in cells leads to the induction of an HSR. To examine this, a suite of constructs was generated for the expression of Cerulean-tagged wild-type SOD1 (SOD1^{WT}), SOD1^{G93A}, Htt^{25Q}, Htt^{72Q}, wild-type Fluc (Fluc^{WT}), or a destabilised mutant (R188Q/R261Q) form of Fluc (Fluc^{DM}; Gupta et al., 2011). These proteins were selected because they represent a mix of: (1) pathogenic (SOD1 and Htt) and non-pathogenic (Fluc) aggregation-prone proteins and their WT isoforms; (2) JUNQ, IPOD, and other inclusion-forming proteins (SOD1, Htt, Fluc, respectively); and (3) amyloidogenic (SOD1 and Htt) and amorphous (Fluc) proteins. Firefly luciferase was chosen because it has no known biological roles in mammalian cells. Moreover, Fluc is widely used in cellular models of protein aggregation because its folding and re-folding is dependent on chaperones (San Gil et al., 2017a; Frydman et al., 1994; Ziętkiewicz et al., 2006).

Cells overexpressing the Cerulean-tagged proteins were analysed by flow cytometry to assess whether the expression of aggregation-prone proteins or their inclusion formation could induce an HSR in Neuro-2a (HSE:EGFP) cells. Cellular debris, doublets, and clumps were excluded from subsequent analyses, as described in Fig. S4. Representative flow cytometric data of the proportion of Cerulean^{+ve} and EGFP^{+ve} cells is shown for cells expressing SOD1^{WT}, SOD1^{G93A}, Htt^{25Q}, Htt^{72Q}, Fluc^{WT}, and Fluc^{DM} (Fig. 3A; comparison of compensated and uncompensated data is shown in Fig. S4). The flow cytometric analysis showed that the proportion of the mCherry-positive population did not vary between the samples (Fig. S4) and the stable expression of mCherry is not differentially affected by overexpression of the various proteins used in this study (Fig. S4). In addition, there were no statistically significant differences between the transfection efficiencies of each of the different plasmids (Fig. S4). There were no statistically significant differences between the overall expression levels of each of the Cerulean-tagged proteins, with the exception of Htt^{72Q}, which demonstrated significantly greater levels of Cerulean fluorescence intensity (P<0.001), likely due to the very large and bright inclusions it forms (Fig. 3C). Expression of the two pathogenic proteins, SOD1^{G93A} or Htt^{72Q}, resulted in 1.6±0.4% and 4.0±1.1% (mean±s.e.m.) of the transfected cells becoming
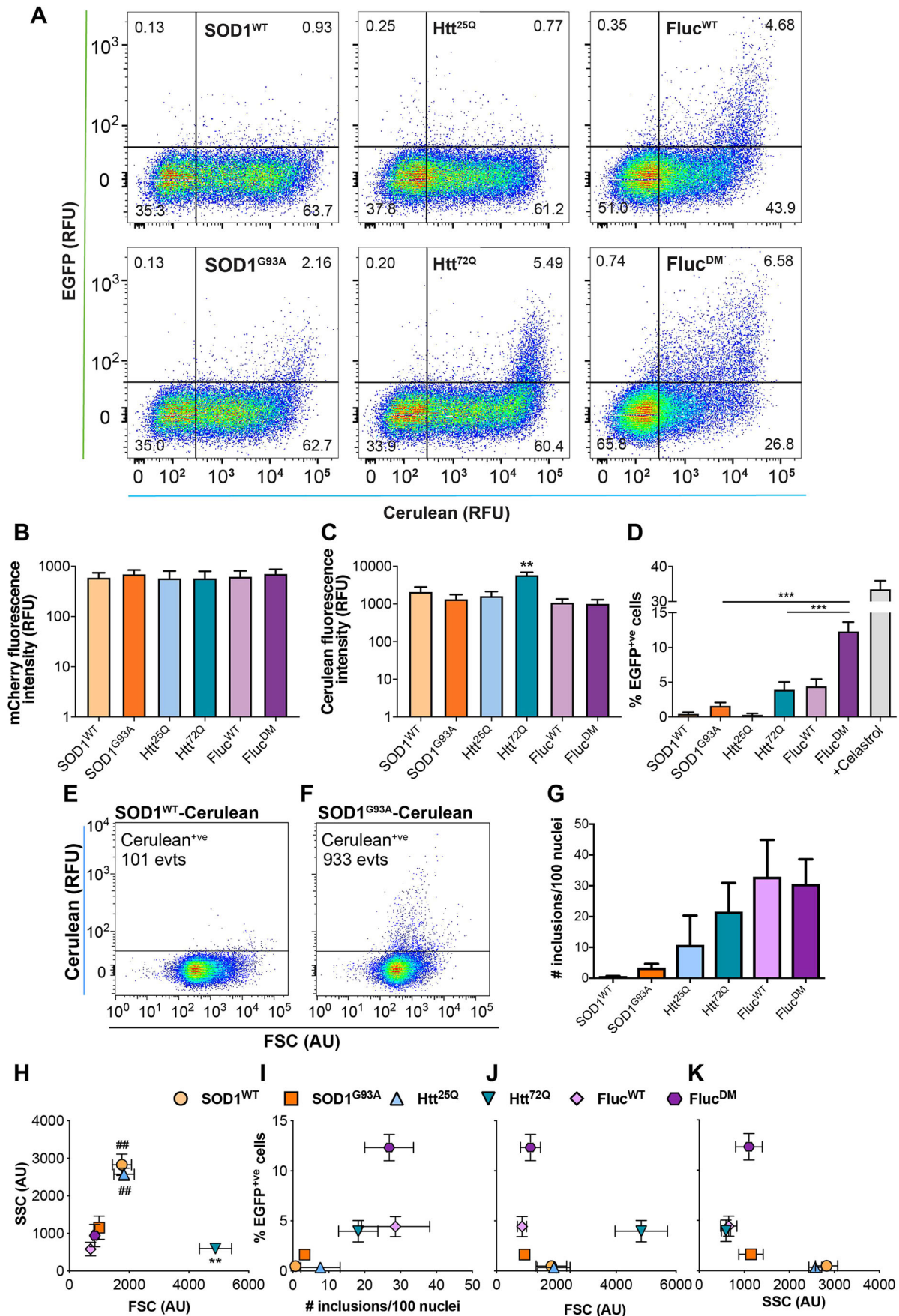
Fig. 3. See next page for legend.

Fig. 3. Overexpression of Fluc^{DM}, but not disease-associated proteins, induces the HSR in Neuro-2a (HSE:EGFP) cells. Neuro-2a (HSE:EGFP) cells were transfected to express Cerulean-tagged SOD1^{WT}, SOD1^{G93A}, Htt^{25Q}, Htt^{72Q}, Fluc^{WT}, or Fluc^{DM} and, 48 h post-transfection, cells were analysed by standard flow cytometry or FloIT. (A–D) Flow cytometric analysis of transfected cells to determine the proportion of cells with an activated HSR. Cellular debris, cell clumps, doublet events and untransfected cells were excluded from the analysis as described in Fig. S4. (A) Representative bivariate plots of EGFP and Cerulean fluorescence of each of the samples. (B) The mCherry fluorescence intensity and (C) Cerulean fluorescence intensity of each of the samples. (D) The proportion of transfected cells expressing Cerulean-tagged WT or mutant proteins that were EGFP^{+ve} and thus have induced an HSR. (E,F) FloIT analysis of cells to determine the relative propensity of each protein to form inclusions in cells. Representative plots of forward scatter (FSC) and Cerulean RFU show events acquired from cells transfected to express (E) SOD1^{WT}–Cerulean and (F) SOD1^{G93A}–Cerulean. The number of Cerulean^{+ve} events are denoted in the gate. (G) The number of Cerulean^{+ve} inclusions quantified by FloIT, normalised to the number of transfected nuclei (total number of nuclei divided by the transfection efficiency of whole cells). (H) Bivariate plot of the FSC (size) and side scatter (SSC; granularity) of the Cerulean^{+ve} inclusions identified by FloIT. The effect of (I) number of inclusions formed, (J) inclusion size (FSC), and (K) inclusion granularity (SSC) on the proportion of cells with an activated HSR (% EGFP^{+ve} cells). Data shown are the mean±s.e.m. of three independent repeats. Statistically significant differences between the means were determined by one-way ANOVA and Tukey's multiple comparisons test. There were no statistically significant differences in B or G. **$P<0.01$ (C, FSC in H); ***$P<0.001$ (D); ##$P<0.01$ (SSC in H).

EGFP^{+ve}, respectively (Fig. 3D). However, this was not significantly different from the proportion of EGFP^{+ve} cells expressing non-aggregation prone isoforms of these proteins (i.e. SOD1^{WT} or Htt^{25Q}). In contrast, the expression of Fluc^{DM} resulted in HSR induction in 12.3±1.3% (mean±s.e.m.) of transfected cells, which was significantly greater than HSR induction in cells expressing the aggregation-prone disease-related proteins (Fig. 3D).

To determine the factors involved in the apparent differential capacity of cells to induce an HSR in the presence of each of the proteins, the propensity of each of these Cerulean-tagged proteins to aggregate was assessed by flow cytometric analysis of inclusions and trafficking (FloIT). FloIT is a flow cytometric method for the quantification of the relative number of fluorescent inclusions formed in cells by analysis of cell lysates (Whiten et al., 2016). A sample without the far-red nuclear stain RedDot1 was used as a negative control to set the gate that defined non-nuclear particles on plots of RedDot1 fluorescence and forward scatter (FSC; Fig. S5). The addition of RedDot1 to cell lysates enabled nuclei to be identified, enumerated, and non-nuclear particles to be further analysed for the quantification of Cerulean^{+ve} inclusions (Fig. S5). Lysates from cells transfected to express SOD1^{WT}, which does not readily form inclusions (McAlary et al., 2016; Whiten et al., 2016), were used as a negative control to set the gates for Cerulean^{+ve} inclusions on plots of Cerulean fluorescence and FSC (Fig. 3E). Cerulean-tagged SOD1^{G93A} formed inclusions, which could be quantified (Fig. 3F), but were relatively few (mean±s.e.m. of 3.2±0.7 inclusions/100 nuclei) compared to Htt^{72Q} (mean±s.e.m. of 18.2±6.3 inclusions/100 nuclei; Fig. 3G). The total number of inclusions formed by each overexpressed protein varied and was highest for Fluc^{WT} and Fluc^{DM}. The relative propensity for each of the proteins tested to form inclusions detectable by FloIT was (in ascending order, least to most); SOD1^{WT}<SOD1^{G93A}<Htt^{25Q}<Htt^{72Q}<Fluc^{DM}<Fluc^{WT} (Fig. 3G). There were no statistically significant differences in the number of aggregates quantified in these samples.

One factor that could possibly influence HSR induction is the size and/or granularity of the inclusions formed by each protein, since this would be an indirect measure of the surface area available to interact with cytoplasmic proteins. FloIT analysis demonstrated that the inclusions formed by Cerulean^{+ve} SOD1^{WT} and Htt^{25Q} had a significantly greater granularity (side scatter, SSC) compared to the other proteins tested ($P<0.01$; Fig. 3H). In addition, the relative size of the inclusions formed by Htt^{72Q} were significantly larger (based on the FSC signal, Fig. 3H) compared to inclusions formed by Fluc^{DM}, Fluc^{WT}, and SOD1^{G93A} [one-way ANOVA, $F(5, 8)=8.027$, $P=0.0056$].

Taken together, the flow cytometric data from whole cells and cell lysates (FloIT) demonstrate that non-pathogenic Fluc^{DM} elicited an HSR in a significantly greater proportion of cells compared to those expressing pathogenic proteins SOD1^{G93A} or Htt^{72Q}. To expand on this finding, correlation analysis was applied to the dataset to determine whether there was a relationship between the proportion of cells in which an HSR was induced and either the number of inclusions or inclusion surface area. There was a trend towards a modest positive linear relationship between the number of inclusions formed by a protein and the proportion of cells with an active HSR, but this was not significant (Fig. 3I; $r=0.77$; $P=0.073$). Moreover, there was not a significant correlation between the size (FSC; $r=-0.13$; $P=0.802$) or granularity (SSC; $r=-0.52$; $P=0.288$) of the inclusions identified by FloIT and the proportion of EGFP^{+ve} cells (Fig. 3J and K, respectively), demonstrating that there is no linear relationship between inclusion surface area and HSR induction in these cells.

Intracellular concentration of aggregation-prone proteins is a significant factor influencing HSR induction

Given that the analysis of the entire cell population by flow cytometry demonstrated that pathogenic SOD1 and Htt did not elicit an HSR in a significant proportion of cells compared to their respective WT proteins, we next sought to determine whether the intracellular expression level of an aggregation-prone protein affects the induction of the HSR. To do so, events from the flow cytometric analyses were binned according to the levels of Cerulean expression [5000 relative fluorescence units (RFU) per bin, where bin one contains cells with the lowest expression and bin ten the highest level of expression; Fig. 4A). Thus, cells in the same Cerulean bin express comparable levels of the protein. In this way, we were able to compare the effect that increasing expression levels of an intracellular protein has on HSR induction across each of the samples. The proportion of cells in each of these bins in which an HSR was induced was determined. Representative bivariate plots of EGFP and FSC of cells transfected to express Htt^{72Q} in Cerulean bins 5 and 10 are shown in Fig. 4B. By binning the flow cytometry data in this way two factors can be assessed: (1) the effect of high and low protein concentration on induction of the HSR, and (2) the induction of the HSR in cells expressing equivalent amounts of WT and mutant aggregation-prone proteins (Fig. 4C–E).

In SOD1^{G93A}–Cerulean-expressing cells, as the amount of SOD1^{G93A} expressed by cells increased so did the proportion of cells in which an HSR had been induced (0.4±0.2% of cells were EGFP^{+ve} in bin 1 compared to 38.7±7.3% of cells in bin 10, mean± s.e.m; Fig. 4C). This same trend was observed for cells expressing Htt^{72Q}, Fluc^{WT} and Fluc^{DM}, that is, cells expressing the highest amounts of these proteins (bin 10) had the highest proportion of EGFP^{+ve} cells (mean±s.e.m. of 23.4±7.6%, 37.1±15.9%, and 57.7± 10%, respectively; Fig. 4D,E). In contrast, overexpression of non-aggregation prone isoforms of SOD1^{WT} and Htt^{25Q} did not induce
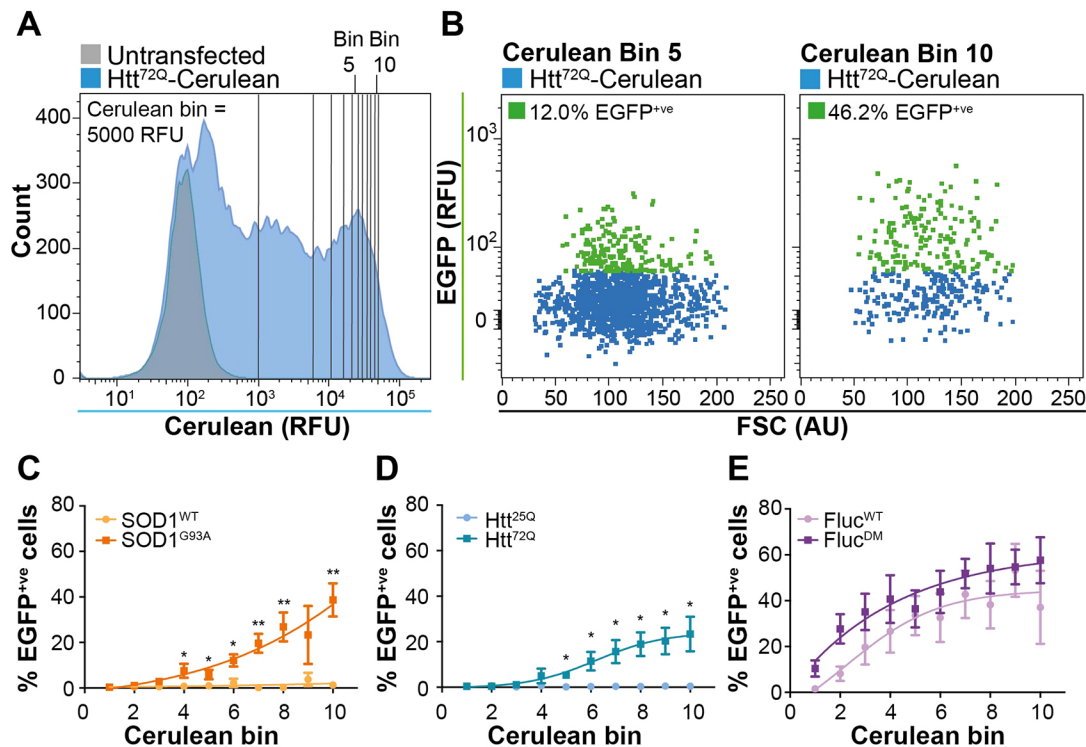
Fig. 4. High expression levels of aggregation-prone proteins correlate with an increase in the proportion of cells with an activated HSR. (A) Overlay histograms of untransfected (grey) and Htt[72Q]–Cerulean (blue) transfected Neuro-2a (HSE:EGFP) cells with ten Cerulean bins corresponding to 5000 RFU each. (B) Representative plots of FSC and EGFP fluorescence from cells transfected to express Htt[72Q]–Cerulean (bin 5, left; bin 10, right). The EGFP[+ve] cells in the indicated Cerulean bin (green) are highlighted. (C–E) The percentage of EGFP[+ve] cells in each Cerulean bin for cells expressing (C) SOD1[WT] or SOD1[G93A], (D) Htt[25Q] or Htt[72Q], or (E) Fluc[WT] or Fluc[DM]. Data shown are the mean±s.e.m. of three independent repeats. Differences between the means were determined using a two-way ANOVA followed by Bonferroni's post hoc test. *$P<0.05$, **$P<0.01$.

an HSR in any Cerulean bin. This demonstrates that it is not simply protein overexpression but also the propensity of the protein to aggregate that induces an HSR in these cells. The HSR was most sensitive to increasing concentrations of Fluc[DM] and Fluc[WT] since, in Cerulean bins 1 and 2, respectively, an EGFP[+ve] population was already evident. There was a significant increase in the proportion of EGFP[+ve] cells in bin 5 and bin 4 for Htt[72Q] and SOD1[G93A], respectively, compared to WT controls. Taken together, these data show that there is a positive relationship between the intracellular levels of aggregation-prone proteins and HSR induction. The same relationship does not exist for proteins that are not aggregation prone (SOD1[WT] and Htt[25Q]). In addition, the HSR is more sensitive to induction at lower relative levels of expression of Fluc[WT] and Fluc[DM] compared to Htt[72Q] and SOD[G93A].

Formation of inclusions precedes the detection of HSR induction and the rate of protein aggregation does not influence HSR induction

Finally, we investigated whether HSR activation occurs before or after inclusion formation in those cells in which inclusions are formed. This was done in order to determine whether HSR induction occurs in response to increasing concentrations of soluble aggregation-prone proteins or as a result of inclusion formation. We used Neuro-2a (HSE:EGFP) cells overexpressing Htt[72Q] or Fluc[DM] for these experiments because inclusions are readily formed in these treatments, yet they have a differential capacity to induce an HSR (Fig. 3D). This is exemplified by the proportion of EGFP[+ve] events in cells expressing Htt[72Q] (mean±s.e.m. of 4.0±1.1%) compared to Fluc[DM] (mean±s.e.m. of 12.3±1.3%; Fig. 3D). Live-cell time-lapse

confocal imaging of Neuro-2a (HSE:EGFP) cells facilitated the simultaneous tracking of Htt[72Q] or Fluc[DM] expression, inclusion formation, and HSR induction in single cells (Fig. 5).

Due to the broad fluorescence emission spectrum of the Cerulean protein, spectral overlap was observed between the channels used to detect EGFP and Cerulean fluorescence, particularly in regions containing inclusions (Fig. S6). To minimise spectral overlap, narrow emission windows for detection of Cerulean and EGFP fluorescence were used when imaging (462–492 nm and 506–563 nm, respectively; Fig. S6). Despite this, an apparent EGFP signal was observed in areas containing inclusions comprised of Cerulean-tagged proteins (areas of intense fluorescence; Fig. S6A inset, white arrowheads), as a result of Cerulean fluorescence being detected in the EGFP emission window.

There was no detectable HSR induction observed at any time point following transfection of cells with Htt[72Q] (Fig. 5, top). In contrast, in cells expressing Fluc[DM], there was an increase in EGFP expression, indicative of HSR induction, in two of the three representative cells depicted after 15 h of incubation (Fig. 5, middle). Treatment with 10 µM CdCl₂ (positive control) resulted in a time-dependent increase in EGFP fluorescence (Fig. 5, bottom), consistent with our data demonstrating induction of an HSR in cells following this treatment (Fig. 1A,C).

Images from these live-cell imaging experiments were subjected to the non-biased image quantification analyses outlined in Fig. S6, to track the expression of Cerulean-tagged proteins, formation of inclusions, and induction of the HSR over time. To accurately measure the level of EGFP over time despite the Cerulean spillover into the EGFP emisssion window, 'cells' and 'inclusions' were
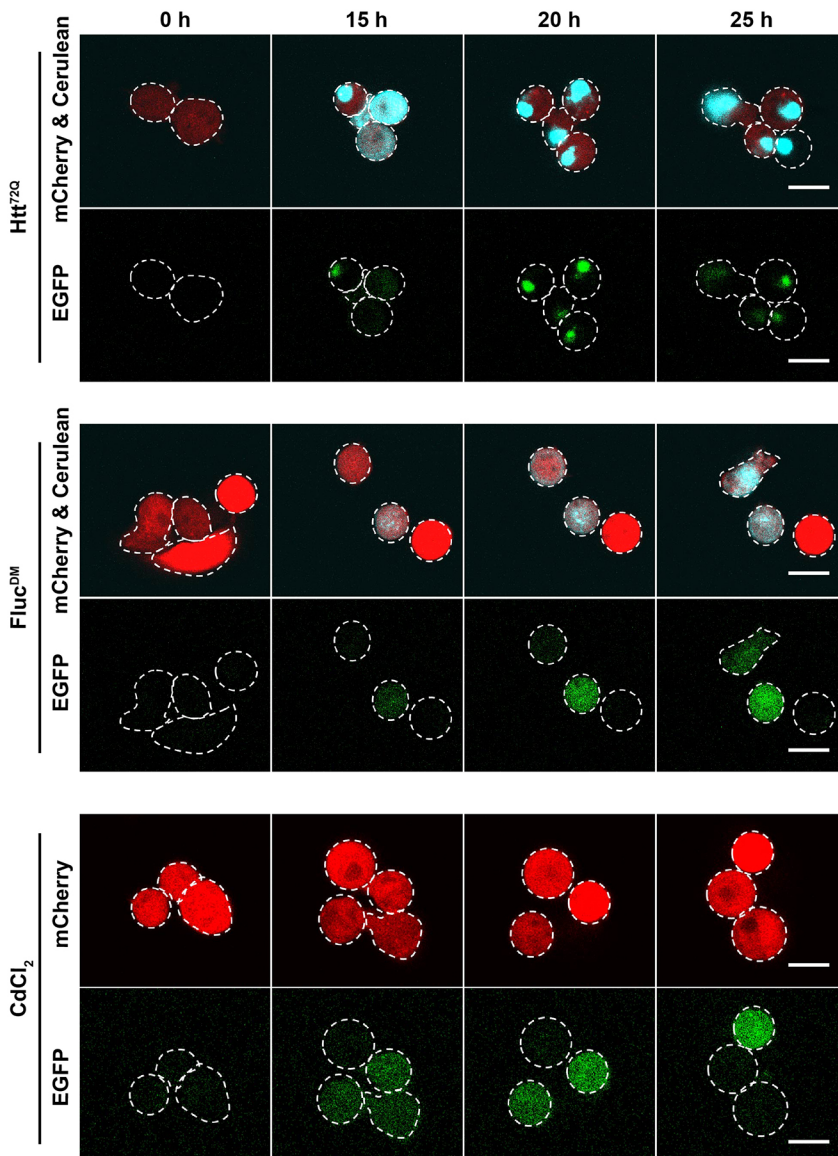
Fig. 5. The induction of the HSR and inclusion body formation captured by live-cell imaging. Neuro-2a (HSE:EGFP) cells were transfected to express Htt^{72Q} (top) or Fluc^{DM} (middle), or treated with 10 μM CdCl$_2$ (bottom) and imaged every hour by confocal microscopy. Representative confocal images are shown after 0, 15, 20 and 25 h of treatment. Each image is overlaid with cell outlines (white dotted line) as defined by the mCherry signal at each time point. The diffuse EGFP fluorescence represents the activation of the HSR; punctate EGFP fluorescence in the Htt^{72Q} sample represents spectral overlap from the Cerulean signal. Scale bars: 20 μm. Images are representative of three independent experiments.

identified based on their mCherry and Cerulean fluorescence, respectively, and EGFP fluorescence intensity was measured from an area in the cell defined as 'cells – inclusions' (Fig. S6). Treatment of Neuro-2a (HSE:EGFP) cells with 10 μM CdCl$_2$ (positive control) resulted in a time-dependent increase in the proportion of cells that were EGFP^{+ve} compared to untreated cells (Fig. 6A). Treatment with CdCl$_2$ significantly increased the proportion of EGFP^{+ve} cells compared to no treatment [two-way ANOVA, F (1, 130)=369.7, $P<0.0001$], and this reached statistical significance 12 h after treatment. Likewise, there was a time-dependent increase in the proportion of cells with an active HSR in samples transfected to express Fluc^{DM} (Fig. 6B). In contrast, there was little or no effect of Htt^{72Q} expression on the proportion of EGFP^{+ve} cells over time, which reflects the relative lack of HSR induction in these cells (Fig. 6B). There was a significantly greater proportion of EGFP^{+ve} cells in samples expressing Fluc^{DM} compared to Htt^{72Q} [two-way ANOVA, F (1, 144)=33.43, $P<0.0001$]. Post hoc analysis using Bonferroni's test showed that this difference was statistically significant 21 h following transfection. Therefore, these data again demonstrate that Fluc^{DM} and Htt^{72Q} have differential capacities to induce the HSR.

To determine whether the difference in HSR induction observed between cells expressing Fluc^{DM} compared to Htt^{72Q} was associated with the rate of protein expression and/or the aggregation rate of these proteins, the Cerulean fluorescence intensity and the proportion of cells with Htt^{72Q} or Fluc^{DM} inclusions was determined over the timecourse of the imaging experiment (Fig. 6C,D). There was a comparable rate of protein synthesis between Htt^{72Q} and Fluc^{DM} as determined by tracking Cerulean fluorescence intensity over time (Fig. 6C). There was a significant time-dependent increase in the number of inclusions formed in Neuro-2a (HSE:EGFP) cells by both Htt^{72Q} and Fluc^{DM}, with both samples reaching a plateau in the proportion of cells with inclusions after 20 h [two-way ANOVA, F (12, 143)=33.43, $P<0.0001$]. There was no effect of the type of protein expressed on the mean proportion of cells with inclusions formed over the time-course of the experiment [two-way ANOVA, F (1, 143)=0.09, $P=0.7607$]. Both Htt^{72Q} and Fluc^{DM} reached half maximal inclusion formation 12.8±2.4 h and 13.9±3.4 h (mean± s.e.m.) following transfection, respectively, indicating that there was no significant difference in the rate of inclusion formation of either protein. Therefore, the rate of inclusion formation of each of these proteins does not influence HSR induction.
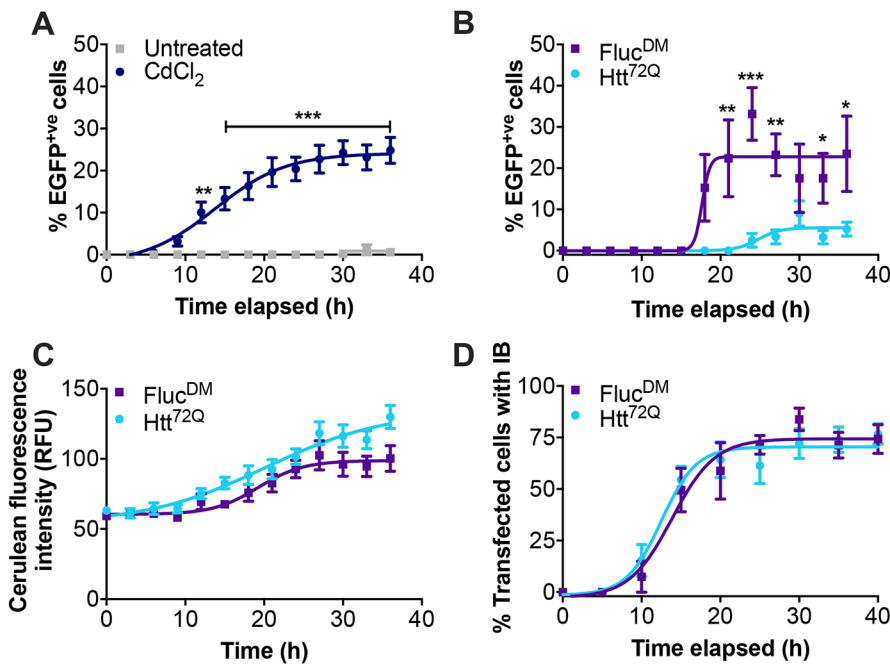
Fig. 6. The induction of the HSR in cells expressing Fluc^{DM} or Htt^{72Q} is not dictated by the rate of aggregate formation. (A) The proportion of EGFP^{+ve} cells over time after treatment (or not) with 10 μM CdCl$_2$. (B) The proportion of EGFP^{+ve} cells over time after transfection to express Htt^{72Q} or Fluc^{DM}. (C) The proportion of Cerulean^{+ve} cells over time after transfection to express Htt^{72Q} or Fluc^{DM}. (D) The proportion of transfected cells with inclusions over time. Data shown are the mean±s.e.m. of single cell analyses of >300 transfected cells from eight fields of view using a 40× dry objective. These findings are representative of three independent live-cell imaging experiments. Differences in the means were assessed using a two-way ANOVA followed by post hoc analysis using Bonferroni's test. *P<0.05, **P<0.01, ***P<0.001.

The first Fluc^{DM} inclusions were detected 10 h after transfection, whereas the first HSR-positive cells were detected 18 h after transfection (i.e. 8 h later). This time delay between when inclusions were first detected and when HSR induction was observed in cells (i.e. when EGFP fluorescence was detected in the cells) likely represents the time taken for HSF1 to activate, translocate to the nucleus, and drive transcription of the EGFP reporter to a level sufficient for detection by the confocal microscope.

One of the limitations of time-lapse image analysis is the inability to detect inclusions of a range of sizes and fluorescence intensities, since the imaging parameters need to be set at the beginning of the experiment (i.e. before the cells exhibit fluorescence). Thus, a trade-off is required between choosing laser power and voltage settings that enable the sensitive detection of fluorescence at early time points following transfection with those needed to ensure signals are not saturated by the inclusions by the end of the experiment. Consequently, it is likely that the reported maximum proportion of cells with inclusions (75% after 25 h for Fluc^{DM} and Htt^{72Q}) is an underestimate. Likewise, it is possible that the reported proportion of EGFP^{+ve} cells is also an underestimate.

DISCUSSION

The HSR is widely recognised as a first line of defence against protein aggregation as it results in the increased expression of molecular chaperones and increased capacity of degradation pathways. However, an explanation as to why molecular chaperones such as the Hsps fail to become upregulated and suppress the formation of protein aggregates in neurodegenerative diseases is lacking. Therefore, we investigated whether protein aggregates are themselves capable of inducing an HSR in a cell line of neuronal origin. In this work, we provide strong evidence that extracellular and intracellular disease-associated protein aggregates are poor inducers of the HSR.

Using a Neuro-2a-derived stable cell line that reports on HSF1 activation, Neuro-2a (HSE:EGFP) cells, we show that the extracellular application of the pathogenic aggregates α-synuclein and SOD1^{G93A} does not result in the induction of an HSR. Intracellular overexpression of the pathogenic proteins Htt^{72Q} and

SOD1^{G93A} induced an HSR in a small, but not significant proportion of cells. In contrast, overexpression of the non-disease related aggregation-prone protein Fluc did result in the induction of an HSR in a significantly greater proportion of cells compared to SOD1^{G93A} and Htt^{72Q}. Moreover, our data demonstrates that there is a positive relationship between the concentration of aggregation-prone proteins and induction of the HSR in cells; higher intracellular concentrations of aggregation-prone proteins lead to HSR induction in a greater proportion of cells. Our study provides evidence that these disease-associated protein aggregates have limited capacity to induce an HSR. As such, therapeutic strategies that activate the HSR, in order to enhance levels of molecular chaperones and restore proteostasis, might be of benefit in these disorders.

The cell-to-cell transfer of protein aggregates through the extracellular medium is thought to be one mechanism by which neurodegenerative diseases progress from a focal point of onset (Scheckel and Aguzzi, 2018). Indeed, both SOD1 and α-synuclein have been shown to act in a prion-like manner in various cell and animal models of disease (McAlary et al., 2019; Leak et al., 2019). In the present study we showed that the extracellular application of SOD1^{G93A} and α-synuclein aggregates to Neuro-2a (HSE:EGFP) cells did not result in an induction of the HSR up to 72 h post-treatment. The absence of an HSR in cells after treatment with protein aggregates suggests that these pathogenic proteins evade detection by the components of the HSR that activate this pathway. Thus, the failure of aggregated SOD1 and α-synuclein to activate the HSR might contribute to disease progression in neurodegenerative diseases by enabling the seeding of inclusions in neighbouring cells that take up aggregates. Future research could investigate the ability of primary astroglia to induce an HSR after application of protein aggregates to the medium in order to determine whether external protein aggregates impair or evade the HSR in HSR-competent cell types of the CNS.

One possible explanation for the observed differences in HSR induction across the different proteins tested could be the intrinsic propensity of the proteins to form amorphous or amyloid inclusions, or alternatively IPOD or JUNQ aggregates. Here we showed that the intracellular expression of the pathogenic proteins, SOD1^{G93A}

(JUNQ) and Htt^{72Q} (IPOD), resulted in a low proportion of cells (2–4% of transfected cells) in which an HSR was induced 48 h after transfection. This suggests that the HSR is not activated by protein misfolding or subsequent inclusion formation in the majority of SOD1^{G93A}- or Htt^{72Q}-expressing cells. Therefore, our data suggests that JUNQ or IPOD inclusions, or the monomeric proteins prone to JUNQ or IPOD formation, are poor inducers of the HSR. Future research should characterise the properties of Fluc inclusions, including the precise nature by which they form in cells, since this might uncover the specific factors responsible for inducing an HSR as proteins aggregate in cells. Interestingly, in vitro, mutant SOD1, α-synuclein, and Htt (Scherzinger et al., 1997) are β-sheet forming, amyloidogenic proteins, whereas Fluc forms amorphous aggregates (Gupta et al., 2011). Therefore, it may be that the off-folding pathway (i.e. amorphous or amyloid aggregation), rather than the subtype of inclusion (i.e. IPOD, JUNQ, or other) is responsible for the observed differences in HSR induction across the different proteins tested. Future studies could further examine this hypothesis by analysing a broader range of proteins that aggregate via amorphous and amyloid pathways to form different types of intracellular inclusions.

Previous research using a HEK293 fluorescent reporter cell line suggested that expression of a pathogenic form of Htt, namely Htt^{91Q}, does not lead to detectable induction of the HSR, irrespective of the expression level or aggregation status of the protein in the cell (Bersuker et al., 2013). Likewise, overexpression of artificial β-sheet-forming proteins in HEK293T cells does not induce the expression of Hsp110, Hsp70 or Hsp27, markers of HSR induction (Olzscha et al., 2011). Moreover, the artificial β-sheet-forming proteins significantly inhibit the induction of the HSR in MG132-treated HEK293 cells (monitored using a Fluc reporter downstream of the *HSPA1A* promoter) (Olzscha et al., 2011). Taken together with the data we present here, these findings suggest a possible common underlying mechanism in neurodegenerative diseases, whereby disease-associated proteins evade or attenuate the HSR, which facilitates inclusion formation and propagation throughout the CNS. Future research that incorporates a range of wild-type and disease-causing aggregation-prone proteins could further establish whether this is HSR evasion or attenuation, and if this is a molecular pathology common to all neurodegenerative diseases.

We hypothesised that the rate of protein aggregation or the surface area of the inclusion exposed to the cytosol could play a significant role in inducing the HSR. Therefore, flow cytometry and live-cell confocal imaging experiments were performed to assess whether the capacity of cells to induce an HSR could be attributed to: (1) the rate of inclusion formation of the protein, (2) the physical properties of the inclusions formed (i.e. size and granularity), and/or (3) the intracellular concentration of the aggregation-prone protein. To our knowledge, this is the first study to report on the effects of each of these factors on the induction of the HSR. Because the proportion of cells expressing Htt^{72Q} that exhibited HSR induction was significantly lower than that of cells expressing Fluc^{DM}, we hypothesised that the rate of inclusion formation could be a key determinant in induction of the HSR. Interestingly, there was no significant difference in the rate at which Htt^{72Q} and Fluc^{DM} formed inclusions. Thus, the rate of inclusion formation does not influence HSR induction in this cell-based model. Another factor possibly influencing HSR induction is the size and granularity of the inclusions formed by each protein, since this is an indirect measure of the surface area available to interact with cytoplasmic proteins, including regulators of the HSR. The recent development of FloIT provided an avenue to assess this because it enables the size and granularity of inclusions to be determined (Whiten et al., 2016). Interestingly, the SOD1^{WT} and Htt^{25Q} aggregates demonstrated significantly greater granularity compared to the other proteins tested. Fluc^{DM} formed inclusions that were significantly smaller than those formed by Htt^{72Q} but were similar in size to those formed by SOD1^{G93A}. Linear regression analysis indicated that neither the size nor granularity of the aggregate influences induction of the HSR in these cells.

High intracellular levels of proteins that exceed their predicted solubility is a key determinant of protein aggregation. This concept of 'supersaturation' is thought to be a significant factor driving protein aggregation in neurodegenerative diseases (Ciryam et al., 2015). Indeed, proteins associated with ALS, such as TDP-43 (TARDBP), FUS and SOD1 are supersaturated in the cell and, in their wild-type form, are susceptible to destabilisation and aggregation under conditions that drive proteostasis imbalance (Ciryam et al., 2017). This instability is exacerbated by familial mutations in proteins linked to neurodegenerative diseases resulting in inherently aggregation-prone, supersaturated proteins in inherited neurodegenerative diseases (Yerbury et al., 2019). Using our Neuro-2a (HSE:EGFP) cells we determined whether increasing concentrations of aggregation-prone proteins (and thus their level of saturation) resulted in induction of the HSR. Our data show that there is a strong positive correlation between the amount of the aggregation-prone protein in cells (SOD1^{G93A}, Htt^{72Q}, Fluc^{DM} and Fluc^{WT}) and HSR induction. Significantly, this correlation was not observed for non-pathogenic forms of these disease-related proteins, which are much less prone to aggregation (SOD1^{WT} and Htt^{25Q}). Thus, the levels of these proteins per se does not drive HSR induction; rather, it is the susceptibility of the protein to aggregation combined with high intracellular levels that influences HSR induction.

Lower concentrations of Fluc^{DM} and Fluc^{WT} were capable of inducing an HSR compared to Htt^{72Q} and SOD1^{G93A} and this could suggest that the form of aggregation (i.e. amorphous versus amyloidogenic) might also be an important factor in HSR induction. The HSR was more sensitive to increasing levels of Fluc^{DM} and Fluc^{WT}, and/or the induction of the HSR was impaired or evaded by Htt^{72Q} and SOD1^{G93A} until a critical concentration was reached. Future research could work towards understanding whether the HSR is triggered in response to high concentrations of the aggregation-prone monomeric/oligomeric protein (i.e soluble) or aggregated forms of protein.

In summary, this work shows that neurodegenerative disease-associated proteins are poor inducers of the HSR. Extracellular protein aggregates fail to induce the HSR in neuronal-like cells. Most remarkably, the intracellular expression of pathogenic aggregation-prone proteins also has a limited capacity to induce an HSR. Uniquely, we were able to determine the effect of a number of different factors pertaining to protein aggregates on HSR induction, including the aggregation propensity of pathogenic and non-pathogenic proteins, the level of the aggregation-prone protein within cells, the number of inclusions formed, the physical properties of the inclusions (size and granularity), and the rate at which inclusions formed. Based on flow cytometric and live-cell imaging data it is concluded that HSR induction is dependent on the susceptibility of the protein to aggregation and high intracellular levels of the aggregation-prone protein. Induction of the HSR was not significantly affected by the number of inclusions formed, inclusion size, nor the rate of inclusion formation. The limited capacity of disease-related protein aggregates to induce an HSR suggests that they may evade detection and could even

potentially impair the HSR. This work provides strong evidence of the shortcomings of endogenous cellular proteostasis mechanisms in responding to protein aggregation events that initiate neurodegenerative diseases. Therefore, it follows that therapeutic approaches that act to induce the HSR in the CNS, to boost levels of molecular chaperones and restore proteostasis, are viable strategies to reduce protein aggregation linked to neurodegenerative disorders.

MATERIALS AND METHODS

All reagents and chemicals used in this work were obtained from Merck-Sigma-Aldrich (NSW, Australia) and Amresco (OH, USA) unless otherwise stated.

Plasmids

To generate cell lines that stably and constitutively express mCherry and stress-inducible EGFP downstream of a minimal Hsp70 promoter (minHsp70p) the following two constructs were generated; pCMV-mCherry and pminHsp70p-EGFP. With respect to pCMV-mCherry, the EGFP gene was excised from pEGFP-N1 (Takara Clontech, France) with flanking *Eco*RI/*Bsr*GI sites and replaced with the mCherry gene. Regarding pminHsp70p-EGFP, a minimal Hsp70 promoter consisting of eight putative heat shock elements (HSE; conserved pentameric sequence, nGAAn) upstream of an EGFP gene was excised with flanking *Acc*651/*Bam*HI sites (kind gift of Dr Franck Couillaud, University of Bordeaux, France and Dr Chrit Moonen, UMC Utrecht, The Netherlands; Fig. S1) and subcloned into *Acc*651/*Bam*HI digested pGL4.4 (Thermo Fisher Scientific, VIC, Australia) containing a hygromycin resistance gene.

The constructs coding for the expression of Cerulean-tagged huntingtin exon 1 fragment (Htt) with a non-pathogenic (i.e. 25 polyglutamines; pT-Rex-Cerulean-Htt^{25Q}) or pathogenic (i.e. 72 polyglutamines; pT-Rex-Cerulean-Htt^{72Q}) polyglutamine tracts were kind gifts from Prof. Danny Hatters (University of Melbourne, VIC, Australia). Constructs for the expression of Cerulean-tagged SOD1^{WT}, SOD1^{G93A}, WT firefly luciferase (Fluc^{WT}) and a double mutant (R188Q/R261Q) form of Fluc (Fluc^{DM}) were also generated. To do so, the *cerulean* gene was PCR amplified from pT-Rex-Htt^{72Q} using forward (5′-catggatccaccggtcgccaccatggtgagca-3′) and reverse (5′-caggattcttacttgtacagctc-3′) primers with flanking *Bam*HI/*Bsr*GI restriction sites to replace the EGFP gene in pEGFP-N1-SOD1^{WT} and pEGFP-N1-SOD1^{G93A}, generated as previously described (Turner et al., 2005) The *cerulean* gene was PCR amplified from pT-Rex-Htt^{72Q} using forward (5′-catgggatccaccggccggtcgccaccatggtgagc-3′) and reverse (5′-caggattcttacttgtacagctc-3′) primers with flanking *Bam*HI/*Bsr*GI restriction sites to replace the EGFP gene in pcDNA4-TO-myc-hisA-EGFP-Fluc^{WT} and pcDNA4-TO-myc-hisA-EGFP-Fluc^{DM} (these constructs were kind gifts of Prof. Mark Wilson, University of Wollongong, NSW, Australia). All the constructs generated and used in this work were verified by sequencing using a Hitachi 3130xl Genetic Analyser (Applied Biosystems, MA, USA).

Generation of SOD1^{G93A} and α-synuclein aggregates
Thioflavin T-based aggregation assays

The formation of SOD1^{G93A} aggregates was monitored by an *in situ* ThT binding assay that has previously been described (McAlary et al., 2016). Briefly, 100 μM purified SOD1^{G93A} was incubated with 20 mM dithiothreitol (DTT), 5 mM EDTA and 10 μM ThT in PBS (pH 7.4) at 37°C. The reaction mixtures were loaded into a clear-bottomed 384-well plate (Greiner, Germany). The plate was incubated in a PolarStar Omega Plate Reader (BMG Labtechnologies, VIC, Australia) at 37°C for 30 min prior to covering with adhesive film and commencing readings of samples. The plate underwent double orbital shaking at 300 rpm for 300 s at the start of a 900 s cycle for at least 200 cycles. The ThT fluorescence was measured by excitation at 450 nm and its emission read at 480 nm using the bottom optic.

The formation of α-synuclein fibrils was determined by an end-point ThT assay as previously described (Buell et al., 2014). Briefly, α-synuclein seeds were produced by incubating 150 μM α-synuclein in 50 mM phosphate buffer (pH 7.4), for 48 h at 40°C under maximal stirring with a magnetic

stirrer (WiseStir MSH-20A, Witeg, Germany). The seed fibrils were fragmented by sonication using a microtip probe sonicator (Branson 250 Digital Sonifer, Branson Ultrasonics, CT, USA), using 30% amplification and three cycles of 10 s pulses. The fibrils were flash frozen in liquid nitrogen and stored at −80°C until required. To produce mature fibrils, 100 μM of monomeric α-synuclein was incubated with 1% (w/w) α-synuclein seeds in 50 mM phosphate buffer (pH 7.4) at 37°C for 72 h. A 5 μl aliquot of the α-synuclein fibrils was then loaded into a black clear-bottomed 384-well plate with 25 μl 50 mM phosphate buffer containing 10 μM ThT. The ThT fluorescence was measured by excitation at 450 nm and its emission read at 480 nm using the bottom optic.

Transmission electron microscopy of SOD1^{G93A} and α-synuclein

TEM was employed to visualise the recombinant SOD1^{G93A} and α-synuclein aggregates. An 8 μl aliquot of the aggregated protein directly from the microplates (see above) was applied onto an ultrathin carbon film-coated 400-mesh copper TEM grid (ProSciTech, QLD, Australia). Samples were then diluted with 2 μl of 0.22 μm filtered milli-Q H$_2$O and left for 3 min. Grids were dried with lint-free paper by wicking away the H$_2$O from the side. Grids were washed with 10 μl of milli-Q H$_2$O, dried again, and 10 μl of 1% (w/v) phosphotungstic acid, the contrast reagent, was added and grids left to incubate for 1 min. The phosphotungstic acid was wicked away and the grids were washed twice with 10 μl of milli-Q H$_2$O. Grids were air dried and imaged at the Australian Institute of Innovative Materials (University of Wollongong) using a JEM-2011 TEM (JEOL, Japan). Images were processed using Digital Micrograph (Gatan, CA, USA).

Cell culture of Neuro-2a

The murine neuroblastoma cell line, Neuro-2a, was obtained from the American Type Culture Collection (VA, USA). All cell lines were cultured in DMEM/F-12 supplemented with 2.5 mM L-glutamine and 10% (v/v) FCS (10% FCS-DMEM/F-12) at 37°C under 5% CO2/95% air in a Heracell 150i CO2 incubator (Thermo Fisher Scientific). Cells were passaged every 2 d or once they had reached 80% confluency. The cells were tested for mycoplasma on receipt of the cell line and quarterly thereafter using the MycoAlert Mycoplasma Detection Kit according to the manufacturer's instructions (Lonza, Basel, Switzerland).

Generation and maintenance of Neuro-2a stable cells

Stable cell lines for the constitutive expression of mCherry and stress-inducible expression of EGFP were generated in Neuro-2a cells. Thus, activation of the HSR (i.e. HSF1 binding to HSEs) after treatment with a stressor could be monitored in cells in real time using EGFP as a fluorescent reporter. Neuro-2a cells were used because they are of neuronal origin, express neuronal markers, and are readily transfected using standard lipid-based protocols.

Neuro-2a were first transfected with LTX Plus (Life Technologies, VIC, Australia; 1 μg DNA, 1 μl PLUS reagent and 3 μl Lipofectamine LTX per well) with *Vsp*I linearised pCMV-mCherry and grown under selective pressure (300 μg/ml G418) for 7 d. Monoclonal mCherry-expressing Neuro-2a cell lines were generated by limiting dilution and subsequent monoclonal expansion. We observed a normally distributed range of mCherry fluorescence intensities from this monoclonal cell line. Monoclonal mCherry-expressing Neuro-2a cell lines were transfected with *Not*I linearised pminHsp70p-EGFP and transfected cells were grown under selective pressure (300 μg/ml G418 and 100 μg/ml hygromycin) for 7 d.

To obtain a polyclonal Neuro-2a cell population with stress-inducible EGFP expression, cells were heat shocked (42°C for 2 h with recovery at 37°C for 6 h), harvested by trypsinisation with 0.25% (w/v) trypsin-EDTA at 37°C for 5 min, washed twice in PBS, and resuspended in FACS buffer [1 mM EDTA, 25 mM HEPES and 0.5% (w/v) BSA in PBS]. These cells were then sorted using an S3e Cell Sorter (Bio-Rad Laboratories, NSW, Australia) equipped with 488 nm and 561 nm lasers. Viable, single cells were resolved based on plots of forward scatter-area versus side scatter-area and forward scatter-area versus forward scatter-height. Subsequently, mCherry^{+ve}/EGFP^{+ve} cells were identified and sorted and maintained in complete medium (10% FCS-DMEM/F-12) supplemented with 1× penicillin/streptomycin to prevent bacterial contamination. These EGFP

HSR reporter cell lines are referred to in this work as Neuro-2a (HSE:EGFP), given that EGFP expression is driven by HSF1 binding to HSEs.

Neuro-2a (HSE:EGFP) cells were maintained under the same conditions as the parental cell lines. Constant selection pressure was achieved by supplementing the media used to culture Neuro-2a (HSE:EGFP) with 300 µg/ml G418 and 100 µg/ml hygromycin.

Cell stress treatments
Heat shock, cadmium chloride, and celastrol treatment assays
Heat shock, cadmium chloride ($CdCl_2$) and celastrol (AdooQ Biosciences, CA, USA) were used to assess the capacity of Neuro-2a cells to induce an HSR. Neuro-2a (HSE:EGFP) cells were seeded at a density of 200,000 cells/ml into 12-well plates. Optimal concentrations of $CdCl_2$ and celastrol were determined in concentration-response assays, whereby cells were either treated with $CdCl_2$ (0–33 µM) or celastrol (0–1 µM) for 24 h. In addition, cells were heat shocked (42°C for 2 h) and allowed to recover for different times at 37°C. After each treatment, Neuro-2a (HSE:EGFP) cells were imaged every 2 h for 24 h using an IncuCyte Live Cell Analysis System (Essen BioScience, MI, USA). The optimal treatment concentrations and times for induction of an HSR in these cells were determined to be 10 µM for 24 h for $CdCl_2$, 0.75 µM for 24 h for celastrol and heat shock at 42°C for 2 h with recovery at 37°C for 24 h (Fig. S2).

As a means of assessing magnitude and kinetics of HSR induction following each treatment, the maximum EGFP fluorescence intensity and time taken to reach half of the EGFP maximum intensity was analysed.

Extracellular aggregation stress assays
Pathogenic protein aggregates were applied extracellularly to Neuro-2a (HSE:EGFP) cells, as described previously (Zeineddine et al., 2017, 2015; Hoffmann et al., 2019; Lee et al., 2008). In each of these studies, fibrillar α-synuclein or aggregated SOD1[G93A] were demonstrated to enter the cell under these conditions; however, this was not specifically addressed in this work since we were focussed on establishing whether the protein aggregates resulted in activation of the HSR when exogenously applied to Neuro-2a (HSE:EGFP). Prior to treatment, soluble non-aggregated α-synuclein and SOD1[G93A] were centrifuged (14,000×g for 30 min at 4°C) to remove any oligomeric seeds that might have spontaneously formed. Aggregated SOD1[G93A] was pelleted (14,000×g for 30 min at 4°C) and resuspended in fresh PBS to eliminate possible cytotoxicity of DTT and EDTA in the assay.

Neuro-2a (HSE:EGFP) cells were seeded at a density of 100,000 cells/ml in a 96-well plate and cultured overnight in 10% FCS DMEM/F12. The following day, medium was refreshed with serum free DMEM/F12 and cells were either treated with buffer alone (50 mM phosphate buffer for α-synuclein or PBS for SOD1[G93A]), monomeric α-synuclein or aggregated α-synuclein (1 µM and 10 µM), or dimeric SOD1[G93A] or aggregated SOD1[G93A] (1 µM and 10 µM) diluted in serum-free DMEM/F12. The concentration of the aggregated α-synuclein and SOD1[G93A] applied to the cells refers to the concentration of the monomer equivalent used to make the resulting fibrils/aggregates. Three wells in each plate were treated with 10 µM $CdCl_2$ as a positive control for HSR induction. Cells were imaged every 2 h for 72 h in an IncuCyte Live Cell Analysis System (Essen BioScience).

Intracellular protein aggregation stress assays
Neuro-2a (HSE:EGFP) cells were transfected with Cerulean-tagged WT and aggregation-prone mutant proteins. Cells were seeded at a density of 100,000 cells/ml in 12-well plates and cultured in 1 ml of 10% FCS DMEM/F12 media overnight. Cells were transfected with DNA–lipid complexes (1 µg DNA, 1 µl PLUS reagent, and 3 µl Lipofectamine LTX per well) for the expression of Cerulean-tagged SOD1[WT], SOD1[G93A], Htt[25Q], Htt[72Q], Fluc[WT], or Fluc[DM].

As controls, parental Neuro-2a were either untransfected, or singly transfected to express EGFP, mCherry or Cerulean fluorescent proteins. These samples were used to set gates for the flow cytometric analysis and to determine the spectral overlap that occurs between these three fluorophores so that spectral compensation could be applied prior to analysis. All analyses of the flow cytometry data were performed using FlowJo (version 10.0.8, Tree Star, OR, USA).

Immunoblot analysis
Following heat shock, cells were harvested, washed twice with PBS, and total cellular protein was extracted by lysis with 2% (w/v) SDS in 0.5 M Tris-HCl, pH 6.8, with 1× Halt protease and phosphatase inhibitors (Thermo Fisher Scientific) and heating at 95°C for 5 min. Bicinchoninic acid assays were performed to determine the protein concentrations of the soluble cell extracts as described elsewhere (Redinbaugh and Turley, 1986). Protein concentrations were adjusted so that equal quantities of total protein (30 µg/well) were loaded onto SDS–PAGE gels [6% (v/v) polyacrylamide for HSF1 and 12% (v/v) polyacrylamide for Hsp70 and α-tubulin] for subsequent immunoblotting. SDS protein extracts were electroblotted onto polyvinylidene difluoride membrane (Bio-Rad) using a standard technique (Towbin et al., 1979). Membranes were blocked with 5% (w/v) non-fat milk in Tris-buffered saline (TBS; 50 mM Tris and 150 mM NaCl, pH 7.5) supplemented with 0.05% (v/v) Tween-20 (TBS-T) for 1 h at room temperature. Membranes were incubated at 4°C overnight with primary antibodies for HSF1 (1:1000; ab81279, Abcam), Hsp70 (1:1000; ADI-SPA-810, Enzo Life Sciences), and α-tubulin (1:10,000; T8203, Sigma-Aldrich). HeLa cells heat shocked at 42°C for 2 h with no recovery were used as a positive control sample for markers of HSR induction. The blots were washed four times for 10 min with TBS-T, incubated with the corresponding horseradish peroxidase (HRP)-conjugated secondary antibody (1:5000) for 1 h at room temperature, and washed again in TBS-T four times for 10 min. The labelled proteins were detected using SuperSignal West Dura Extended Duration Chemiluminescent Substrate (Thermo Fisher Scientific) and imaged using an Amersham GelImager600 (GE Healthcare Life Sciences).

IncuCyte Zoom imaging and image analysis
Image analysis of total image fluorescence intensity
Time-lapse fluorescence intensity data from Neuro-2a (HSE:EGFP) cells were acquired using an IncuCyte Live Cell Analysis System. Phase contrast and fluorescence images were acquired at 2 h intervals with the 10× or 20× objective. The fluorescence intensity of mCherry and stress-inducible EGFP were quantified using the basic analyser algorithm (Table S1) from a minimum of nine images per well at each time point. Spectral overlap from the mCherry (3%) channel was removed from the EGFP channel in these images.

The mean EGFP relative fluorescence intensity (RFU) was normalised by dividing the EGFP RFU by the mCherry RFU at each time point to account for relative changes in cell density over time (equation 1). The normalised EGFP data is presented as the mean fold change (Δ) in the EGFP:mCherry ratio (± s.e.m.) of three independent repeats as described by Eqn 2, where $EGFP_{Tx}$ represents the EGFP RFU at any time and $EGFP_{T0}$ represents the EGFP RFU at 0 h.

$$\left(\frac{EGFP\ (RFU)}{mCherry\ (RFU)} \right) = Normalised\ EGFP \qquad (1)$$

$$\left(\frac{Normalised\ EGFP_{Tx}}{Normalised\ EGFP_{T0}} \right) = Fold\ \Delta\ EGFP \qquad (2)$$

Image analysis of single cell fluorescent intensities
Neuro-2a (HSE:EGFP) cells were either left untransfected or transfected to express Htt[72Q] or Fluc[DM] in an eight-well Ibidi chamber (Ibidi, Germany), and imaged on a Leica SP5 confocal microscope at 37°C under 5% CO_2/95% air. High-resolution images were captured using a 63× water immersion objective (NA 1.2) and widefield images were captured using a 40× (NA 0.9) air objective (see Fig. S6 for excitation and emission collection windows). Each well was imaged at eight regions of interest at 1 h intervals for up to 60 h. The imaging parameters (detector voltage, line averaging, laser power, and windows for emission collection) were set at the beginning of this time-lapse experiment and remained constant over the entire period in which cells were imaged. The data obtained were analysed using CellProfiler 2.2.0 (McQuin et al., 2018; Carpenter et al., 2006; Kamentsky et al., 2011). The mask parameters used for the identification of

'cells' and 'inclusions' are outlined in Table S2. These parameters were optimised to separate cell clumps and identify individual cells and inclusions. Using these parameters, the following custom-made sequence of image processing events was used to analyse all images in a non-biased manner: (1) 'cells' were identified as primary objects (Table S2), (2) 'inclusions' were identified as primary objects (Table S2), (3) the region of the cell cytoplasm excluding the inclusions was defined as 'cells – inclusions' tertiary objects, (4) the Cerulean fluorescence intensities of 'cells' and EGFP fluorescence intensities of the regions defined as 'cells – inclusions' was measured. The tertiary objects identified, 'cells – inclusions', were applied to eliminate the spectral overlap between the Cerulean fluorescence signal at the site of inclusions and the EGFP fluorescence signal. In this way EGFP fluorescence was measured from an area of the cell that did not contain inclusion bodies (i.e. 'cells – inclusions').

Bivariate plots of the Cerulean and EGFP fluorescence intensities derived from regions defined as 'cells – inclusions' demonstrated a strong correlation, suggesting that the Cerulean signal was still contributing to the EGFP signal (Fig. S6). This spectral overlap was calculated to be 13% based on EGFP- and Cerulean-only controls. Therefore, spectral compensation was performed on the EGFP data according to Eqn 3.

$$Raw\ EGFP - \left(\frac{Raw\ Cerulean}{1} \times \frac{13}{100}\right) = Corrected\ EGFP \quad (3)$$

Lastly, thresholding was used to count the number of Cerulean^{+ve} (or transfected) cells or EGFP^{+ve} (or HSR^{+ve}) cells at each time point. These thresholds were determined from the EGFP RFU and Cerulean RFU of cells in the untransfected and untreated samples (in this case 65 RFU and 15 RFU, respectively).

Flow cytometric analysis
Analysis of whole cells
Flow cytometry was performed using an LSR Fortessa X-20 cell analyser equipped with 405 nm, 488 nm, 561 nm and 640 nm lasers (BD Biosciences, CA, USA). A minimum of 20,000 events per sample were collected at a high flow rate. Forward scatter was collected using a linear scale and side scatter using a log scale. Fluorescence emissions were collected as area (log scale), pulse height (log scale), and pulse width (linear scale) for each channel. For Cerulean fluorescence, data was collected with the 405 nm laser and 450/50 nm filter, EGFP was collected with the 488 nm laser and 525/50 nm filter, mCherry was collected with the 561 nm laser and 586/15 nm filter, and RedDot1 was collected with the 640 nm laser and 670/30 nm filter. Spectral compensation, gating and data analysis of events acquired by flow cytometry was performed using Flow Jo software (Tree Star). The compensation matrix used for these samples is outlined in Table S3.

Flow cytometric analysis of inclusions and trafficking
The relative aggregation propensity of each of the proteins used in this study was quantified using the FloIT method described elsewhere (Whiten et al., 2016). Briefly, cells to be analysed were grown and transfected in 24-well plates. Cells were washed twice with PBS (pH 7.4) 48 h post-transfection, harvested mechanically by aspiration on ice and resuspended in 500 μl ice-cold PBS for analysis of intact cells (used to quantify transfection efficiency) or cell lysates (used to quantify number of nuclei and Cerulean-positive inclusions) by flow cytometry. An aliquot of the cell suspension (150 μl) was taken and the transfection efficiency determined using untransfected cells as a negative control sample. The remaining 350 μl of cell suspension was lysed, as described previously (Whiten et al., 2016), in PBS containing a final concentration of 0.5% (v/v) TritonX-100 and 1× Halt protease and phosphatase inhibitors. With the exception of the control samples used to set the gates, RedDot1 (Biotium, CA, USA) was diluted 1:1000 into lysis buffer prior to adding to cells. After 2 min incubation at room temperature to lyse cells, the lysate was analysed by flow cytometry measuring forward and side scatter, together with RedDot1 and Cerulean fluorescence. Analysis of all events was performed using Flow Jo (Tree

Star). The number of inclusions per 100 transfected nuclei was calculated according Eqn 4 (Whiten et al., 2016):

$$i = 100\left(\frac{n_i}{y.n_{nuc}}\right) \quad (4)$$

Where i represents the number of inclusions per 100 nuclei, n_i is the number of inclusions detected, y is the transfection efficiency, and n_{nuc} is the number of nuclei counted.

Statistics
Results shown are the mean±s.e.m. of three independent experiments unless otherwise indicated. Evaluation of statistical differences between the means of groups was determined by a one-way ANOVA or two-way ANOVA for multiple comparisons. The F-statistic from the ANOVA test and its associated degrees of freedom (between groups and within groups, respectively) are reported in parentheses. The P-value from the ANOVA test is also stated. Post hoc testing for differences between means was done using Dunnett's test when comparing means to the mean of the control, Tukey's test for multiple comparisons of the means, or Bonferroni's test for comparing the differences in the means between two samples over time, using GraphPad Prism 5 (GraphPad Software, Inc., CA, USA) and as described in the appropriate figure legends. For data showing the fold change in EGFP expression over time in Neuro-2a (HSE:EGFP) cells, a non-linear fit was applied [log(agonist) versus response (Variable slope)] to the data. The time taken to reach half maximal EGFP intensity was determined by using the logEC50 value as a measure of the kinetics of the HSR. For data where the correlation between x and y are analysed, the Pearson's correlation coefficient (r) and P-value (P) are stated.

References
Amin, J., Ananthan, J. and Voellmy, R. (1988). Key features of heat shock regulatory elements. *Mol. Cell. Biol.* **8**, 3761-3769. doi:10.1128/MCB.8.9.3761

Batulan, Z., Shinder, G. A., Minotti, S., He, B. P., Doroudchi, M. M., Nalbantoglu, J., Strong, M. J. and Durham, H. D. (2003). High threshold for induction of the stress response in motor neurons is associated with failure to activate HSF1. *J. Neurosci.* **23**, 5789-5798. doi:10.1523/JNEUROSCI.23-13-05789.2003

Bersuker, K., Hipp, M. S., Calamini, B., Morimoto, R. I. and Kopito, R. R. (2013). Heat shock response activation exacerbates inclusion body formation in a cellular

model of Huntington disease. *J. Biol. Chem.* **288**, 23633-23638. doi:10.1074/jbc.C113.481945

Bolognesi, B., Kumita, J. R., Barros, T. P., Esbjorner, E. K., Luheshi, L. M., Crowther, D. C., Wilson, M. R., Dobson, C. M., Favrin, G. and Yerbury, J. J. (2010). ANS binding reveals common features of cytotoxic amyloid species. *ACS Chem. Biol.* **5**, 735-740. doi:10.1021/cb1001203

Braak, H., Del Tredici, K., Rüb, U., De Vos, R. A. I., Jansen Steur, E. N. H. and Braak, E. (2003). Staging of brain pathology related to sporadic Parkinson's disease. *Neurobiol. Aging* **24**, 197-211. doi:10.1016/S0197-4580(02)00065-9

Braak, H., Alafuzoff, I., Arzberger, T., Kretzschmar, H. and Del Tredici, K. (2006). Staging of Alzheimer disease-associated neurofibrillary pathology using paraffin sections and immunocytochemistry. *Acta Neuropathol.* **112**, 389-404. doi:10.1007/s00401-006-0127-z

Brettschneider, J., Del Tredici, K., Toledo, J. B., Robinson, J. L., Irwin, D. J., Grossman, M., Suh, E. R., Van Deerlin, V. M., Wood, E. M., Baek, Y. et al. (2013). Stages of pTDP-43 pathology in amyotrophic lateral sclerosis. *Ann. Neurol.* **74**, 20-38. doi:10.1002/ana.23937

Brettschneider, J., Arai, K., Del Tredici, K., Toledo, J. B., Robinson, J. L., Lee, E. B., Kuwabara, S., Shibuya, K., Irwin, D. J., Fang, L. et al. (2014). TDP-43 pathology and neuronal loss in amyotrophic lateral sclerosis spinal cord. *Acta Neuropathol.* **128**, 423-437. doi:10.1007/s00401-014-1299-6

Buell, A. K., Galvagnion, C., Gaspar, R., Sparr, E., Vendruscolo, M., Knowles, T. P. J., Linse, S. and Dobson, C. M. (2014). Solution conditions determine the relative importance of nucleation and growth processes in alpha-synuclein aggregation. *Proc. Natl. Acad. Sci. USA* **111**, 7671-7676. doi:10.1073/pnas.1315346111

Carpenter, A. E., Jones, T. R., Lamprecht, M. R., Clarke, C., Kang, I., Friman, O., Guertin, D. A., Chang, J., Lindquist, R. A., Moffat, J. et al. (2006). CellProfiler: image analysis software for identifying and quantifying cell phenotypes. *Genome Biol.* **7**, R100. doi:10.1186/gb-2006-7-10-r100

Chen, H.-J., Mitchell, J. C., Novoselov, S., Miller, J., Nishimura, A. L., Scotter, E. L., Vance, C. A., Cheetham, M. E. and Shaw, C. E. (2016). The heat shock response plays an important role in TDP-43 clearance: evidence for dysfunction in amyotrophic lateral sclerosis. *Brain* **139**, 1417-1432. doi:10.1093/brain/aww028

Chiti, F. and Dobson, C. M. (2017). Protein misfolding, amyloid formation, and human disease: a summary of progress over the last decade. *Ann. Rev. Biochem.* **86**, 27-68. doi:10.1146/annurev-biochem-061516-045115

Ciryam, P., Kundra, R., Morimoto, R. I., Dobson, C. M. and Vendruscolo, M. (2015). Supersaturation is a major driving force for protein aggregation in neurodegenerative diseases. *Trends Pharmacol. Sci.* **36**, 72-77. doi:10.1016/j.tips.2014.12.004

Ciryam, P., Lambert-Smith, I. A., Bean, D. M., Freer, R., Cid, F., Tartaglia, G. G., Saunders, D. N., Wilson, M. R., Oliver, S. G., Morimoto, R. I. et al. (2017). Spinal motor neuron protein supersaturation patterns are associated with inclusion body formation in ALS. *Proc. Natl. Acad. Sci. USA* **114**, E3935-E3943. doi:10.1073/pnas.1613854114

Corish, P. and Tyler-Smith, C. (1999). Attenuation of green fluorescent protein half-life in mammalian cells. *Protein Eng.* **12**, 1035-1040. doi:10.1093/protein/12.12.1035

Cox, D. and Ecroyd, H. (2017). The small heat shock proteins αB-crystallin (HSPB5) and Hsp27 (HSPB1) inhibit the intracellular aggregation of α-synuclein. *Cell Stress Chaperon* **22**, 589-600. doi:10.1007/s12192-017-0785-x

Farrawell, N. E., Lambert-Smith, I. A., Warraich, S. T., Blair, I. P., Saunders, D. N., Hatters, D. M. and Yerbury, J. J. (2015). Distinct partitioning of ALS associated TDP-43, FUS and SOD1 mutants into cellular inclusions. *Sci. Rep.* **5**, 13416. doi:10.1038/srep13416

Frydman, J., Nimmesgern, E., Ohtsuka, K. and Hartl, F. U. (1994). Folding of nascent polypeptide chains in a high molecular mass assembly with molecular chaperones. *Nature* **370**, 111-117. doi:10.1038/370111a0

Fujimoto, M., Takaki, E., Hayashi, T., Kitaura, Y., Tanaka, Y., Inouye, S. and Nakai, A. (2005). Active HSF1 significantly suppresses polyglutamine aggregate formation in cellular and mouse models. *J. Biol. Chem.* **280**, 34908-34916. doi:10.1074/jbc.M506288200

Gupta, R., Kasturi, P., Bracher, A., Loew, C., Zheng, M., Villella, A., Garza, D., Hartl, F. U. and Raychaudhuri, S. (2011). Firefly luciferase mutants as sensors of proteome stress. *Nat. Methods* **8**, 879-884. doi:10.1038/nmeth.1697

Hanspal, M. A., Dobson, C. M., Yerbury, J. J. and Kumita, J. R. (2017). The relevance of contact-independent cell-to-cell transfer of TDP-43 and SOD1 in amyotrophic lateral sclerosis. *Biochim. Biophys. Acta* **1863**, 2762-2771. doi:10.1016/j.bbadis.2017.07.007

Hay, D. G. and Sathasivam, K. (2004). Progressive decrease in chaperone protein levels in a mouse model of Huntington's disease and induction of stress proteins as a therapeutic approach. *Hum. Mol. Genet.* **13**, 1389-1405. doi:10.1093/hmg/ddh144

Heemskerk, J. and Tobin, A. J. (2002). Teaching old drugs new tricks. *Trends Neurosci.* **25**, 494-496. doi:10.1016/S0166-2236(02)02236-1

Hipp, M. S., Kasturi, P. and Hartl, F. U. (2019). The proteostasis network and its decline in ageing. *Nat. Rev. Mol. Cell Biol.* **20**, 421-435. doi:10.1038/s41580-019-0101-y

Hoffmann, A. C., Minakaki, G., Menges, S., Salvi, R., Savitskiy, S., Kazman, A., Vicente Miranda, H., Mielenz, D., Klucken, J., Winkler, J. et al. (2019). Extracellular aggregated alpha synuclein primarily triggers lysosomal dysfunction in neural cells prevented by trehalose. *Sci. Rep.* **9**, 544. doi:10.1038/s41598-018-35811-8

Jucker, M. and Walker, L. C. (2013). Self-propagation of pathogenic protein aggregates in neurodegenerative diseases. *Nature* **501**, 45-51. doi:10.1038/nature12481

Kaganovich, D., Kopito, R. and Frydman, J. (2008). Misfolded proteins partition between two distinct quality control compartments. *Nature* **454**, 1088-1095. doi:10.1038/nature07195

Kakkar, V., Meister-Broekema, M., Minoia, M., Carra, S. and Kampinga, H. H. (2014). Barcoding heat shock proteins to human diseases: looking beyond the heat shock response. *Dis. Model. Mech.* **7**, 421-434. doi:10.1242/dmm.014563

Kamentsky, L., Jones, T. R., Fraser, A., Bray, M.-A., Logan, D. J., Madden, K. L., Ljosa, V., Rueden, C., Eliceiri, K. W. and Carpenter, A. E. (2011). Improved structure, function and compatibility for CellProfiler: modular high-throughput image analysis software. *Bioinformatics* **27**, 1179-1180. doi:10.1093/bioinformatics/btr095

Kayatekin, C., Matlack, K. E., Hesse, W. R., Guan, Y., Chakrabortee, S., Russ, J., Wanker, E. E., Shah, J. V. and Lindquist, S. (2014). Prion-like proteins sequester and suppress the toxicity of huntingtin exon 1. *Proc. Natl. Acad. Sci. USA* **111**, 12085-12090. doi:10.1073/pnas.1412504111

Kopito, R. R. (2000). Aggresomes, inclusion bodies and protein aggregation. *Trends Cell Biol.* **10**, 524-530. doi:10.1016/S0962-8924(00)01852-3

Leak, R. K. (2014). Heat shock proteins in neurodegenerative disorders and aging. *J. Cell Commun. Signal* **8**, 293-310. doi:10.1007/s12079-014-0243-9

Leak, R. K., Frosch, M. P., Beach, T. G. and Halliday, G. M. (2019). Alpha-synuclein: prion or prion-like? *Acta Neuropathol.* **138**, 509-514. doi:10.1007/s00401-019-02057-1

Lee, H.-J., Suk, J.-E., Bae, E.-J., Lee, J.-H., Paik, S. R. and Lee, S.-J. (2008). Assembly-dependent endocytosis and clearance of extracellular a-synuclein. *Int. J. Biochem. Cell Biol.* **40**, 1835-1849. doi:10.1016/j.biocel.2008.01.017

Leitman, J., Ulrich Hartl, F. and Lederkremer, G. Z. (2013). Soluble forms of polyQ-expanded huntingtin rather than large aggregates cause endoplasmic reticulum stress. *Nat. Commun.* **4**, 2753. doi:10.1038/ncomms3753

Lin, P.-Y., Simon, S. M., Koh, W., Folorunso, O., Umbaugh, C. S. and Pierce, A. (2013). Heat shock factor 1 over-expression protects against exposure of hydrophobic residues on mutant SOD1 and early mortality in a mouse model of amyotrophic lateral sclerosis. *Mol. Neurodegener* **8**, 43-43. doi:10.1186/1750-1326-8-43

Matsumoto, G. and Kim, S. (2006). Huntingtin and mutant SOD1 form aggregate structures with distinct molecular properties in human cells. *J. Biol. Chem.* **281**, 4477-4485. doi:10.1074/jbc.M509201200

McAlary, L., Aquilina, J. A. and Yerbury, J. J. (2016). Susceptibility of mutant SOD1 to form a destabilized monomer predicts cellular aggregation and toxicity but not in vitro aggregation propensity. *Front. Neurosci.* **10**, 499. doi:10.3389/fnins.2016.00499

McAlary, L., Plotkin, S. S., Yerbury, J. J. and Cashman, N. R. (2019). Prion-like propagation of protein misfolding and aggregation in amyotrophic lateral sclerosis. *Front. Mol. Neurosci.* **12**, 262. doi:10.3389/fnmol.2019.00262

McQuin, C., Goodman, A., Chernyshev, V., Kamentsky, L., Cimini, B. A., Karhohs, K. W., Doan, M., Ding, L., Rafelski, S. M., Thirstrup, D. et al. (2018). CellProfiler 3.0: Next-generation image processing for biology. *PLoS Biol.* **16**, e2005970. doi:10.1371/journal.pbio.2005970

Mimoto, T., Morimoto, N., Miyazaki, K., Kurata, T., Sato, K., Ikeda, Y. and Abe, K. (2012). Expression of heat shock transcription factor 1 and its downstream target protein T-cell death associated gene 51 in the spinal cord of a mouse model of amyotrophic lateral sclerosis. *Brain Res.* **1488**, 123-131. doi:10.1016/j.brainres.2012.10.012

Montibeller, L. and De Belleroche, J. (2018). Amyotrophic lateral sclerosis (ALS) and Alzheimer's disease (AD) are characterised by differential activation of ER stress pathways: focus on UPR target genes. *Cell Stress Chaperone* **23**, 897-912. doi:10.1007/s12192-018-0897-y

Montibeller, L., Tan, L. Y., Kim, J. K., Paul, P. and de Belleroche, J. (2020). Tissue-selective regulation of protein homeostasis and unfolded protein response signalling in sporadic ALS. *J. Cell. Mol. Med.* **00**, 1-15. doi:10.1111/jcmm.15170

Olzscha, H., Schermann, S. M., Woerner, A. C., Pinkert, S., Hecht, M. H., Tartaglia, G. G., Vendruscolo, M., Hayer-Hartl, M., Hartl, F. U. and Vabulas, R. M. (2011). Amyloid-like aggregates sequester numerous metastable proteins with essential cellular functions. *Cell* **144**, 67-78. doi:10.1016/j.cell.2010.11.050

Pelham, H. R. (1982). A regulatory upstream promoter element in the Drosophila Hsp 70 heat-shock gene. *Cell* **30**, 517-528. doi:10.1016/0092-8674(82)90249-5

Peng, C., Trojanowski, J. Q. and Lee, V. M.-Y. (2020). Protein transmission in neurodegenerative disease. *Nat. Rev. Neurol.* **16**, 199-212. doi:10.1038/s41582-020-0333-7

Polling, S., Mok, Y. F., Ramdzan, Y. M., Turner, B. J., Yerbury, J. J., Hill, A. F. and Hatters, D. M. (2014). Misfolded polyglutamine, polyalanine, and superoxide dismutase 1 aggregate via distinct pathways in the cell. *J. Biol. Chem.* **289**, 6669-6680. doi:10.1074/jbc.M113.520189

Redinbaugh, M. G. and Turley, R. B. (1986). Adaptation of the bicinchoninic acid protein assay for use with microtiter plates and sucrose gradient fractions. *Anal. Biochem.* **153**, 267-271. doi:10.1016/0003-2697(86)90091-6

San Gil, R., Berg, T. and Ecroyd, H. (2017a). Using bicistronic constructs to evaluate the chaperone activities of heat shock proteins in cells. *Sci. Rep.* **7**, 2387. doi:10.1038/s41598-017-02459-9

San Gil, R., Ooi, L., Yerbury, J. J. and Ecroyd, H. (2017b). The heat shock response in neurons and astroglia and its role in neurodegenerative diseases. *Mol. Neurodegener* **12**, 65. doi:10.1186/s13024-017-0208-6

Scheckel, C. and Aguzzi, A. (2018). Prions, prionoids and protein misfolding disorders. *Nat. Rev. Genet.* **19**, 405-418. doi:10.1038/s41576-018-0011-4

Scherzinger, E., Lurz, R., Turmaine, M., Mangiarini, L., Hollenbach, B., Hasenbank, R., Bates, G. P., Davies, S. W., Lehrach, H. and Wanker, E. E. (1997). Huntingtin-encoded polyglutamine expansions form amyloid-like protein aggregates in vitro and in vivo. *Cell* **90**, 549-558. doi:10.1016/S0092-8674(00)80514-0

Sorger, P., Lewis, M. and Pelham, H. R. B. (1987). Heat shock factor is regulated differently in yeast and HeLa cells. *Nature* **329**, 81-84. doi:10.1038/329081a0

Towbin, H., Staehelin, T. and Gordon, J. (1979). Electrophoretic transfer of proteins from polyacrylamide gels to nitrocellulose sheets: procedure and some applications. *Proc. Natl. Acad. Sci. USA* **76**, 4350-4354. doi:10.1073/pnas.76.9.4350

Turner, B. J., Atkin, J. D., Farg, M. A., Zang, D. W., Rembach, A., Lopes, E. C., Patch, J. D., Hill, A. F. and Cheema, S. S. (2005). Impaired extracellular secretion of mutant superoxide dismutase 1 associates with neurotoxicity in familial amyotrophic lateral sclerosis. *J. Neurosci.* **25**, 108-117. doi:10.1523/JNEUROSCI.4253-04.2005

Vaquer-Alicea, J. and Diamond, M. I. (2019). Propagation of protein aggregation in neurodegenerative diseases. *Annu. Rev. Biochem.* **88**, 785-810. doi:10.1146/annurev-biochem-061516-045049

Victoria, G. S. and Zurzolo, C. (2017). The spread of prion-like proteins by lysosomes and tunneling nanotubes: Implications for neurodegenerative diseases. *J. Cell Biol.* **216**, 2633-2644. doi:10.1083/jcb.201701047

Wang, J., Martin, E., Gonzales, V., Borchelt, D. R. and Lee, M. K. (2008). Differential regulation of small heat shock proteins in transgenic mouse models of neurodegenerative diseases. *Neurobiol. Aging* **29**, 586-597. doi:10.1016/j.neurobiolaging.2006.11.009

Webster, J. M., Darling, A. L., Uversky, V. N. and Blair, L. J. (2019). Small heat Shock proteins, big impact on protein aggregation in neurodegenerative disease. *Front. Pharmacol.* **10**, 1047. doi:10.3389/fphar.2019.01047

Westerheide, S. D., Bosman, J. D., Mbadugha, B. N. A., Kawahara, T. L. A., Matsumoto, G., Kim, S., Gu, W., Devlin, J. P., Silverman, R. B. and Morimoto, R. I. (2004). Celastrols as inducers of the heat shock response and cytoprotection. *J. Biol. Chem.* **279**, 56053-56060. doi:10.1074/jbc.M409267200

Whiten, D. R., San Gil, R., McAlary, L., Yerbury, J. J., Ecroyd, H. and Wilson, M. R. (2016). Rapid flow cytometric measurement of protein inclusions and nuclear trafficking. *Sci. Rep.* **6**, 31138. doi:10.1038/srep31138

Winner, B., Jappelli, R., Maji, S. K., Desplats, P. A., Boyer, L., Aigner, S., Hetzer, C., Loher, T., Vilar, M., Campioni, S. et al. (2011). In vivo demonstration that α-synuclein oligomers are toxic. *Proc. Natl. Acad. Sci. USA* **108**, 4194-4199. doi:10.1073/pnas.1100976108

Xiao, H. and Lis, J. (1988). Germline transformation used to define key features of heat-shock response elements. *Science* **239**, 1139-1142. doi:10.1126/science.3125608

Yerbury, J. J., Ooi, L., Dillin, A., Saunders, D. N., Hatters, D. M., Beart, P. M., Cashman, N. R., Wilson, M. R. and Ecroyd, H. (2016). Walking the tightrope: Proteostasis and neurodegenerative disease. *J. Neurochem.* **137**, 489-505. doi:10.1111/jnc.13575

Yerbury, J. J., Ooi, L. Blair, I. P., Ciryam, P., Dobson, C. M. and Vendruscolo, M. (2019). The metastability of the proteome of spinal motor neurons underlies their selective vulnerability in ALS. *Neurosci. Lett.* **704**, 89-94. doi:10.1016/j.neulet.2019.04.001

Zeineddine, R. and Yerbury, J. J. (2015). The role of macropinocytosis in the propagation of protein aggregation associated with neurodegenerative diseases. *Front. Physiol.* **6**, 277. doi:10.3389/fphys.2015.00277

Zeineddine, R., Pundavela, J. F., Corcoran, L., Stewart, E. M., Do-Ha, D., Bax, M., Guillemin, G., Vine, K. L., Hatters, D. M., Ecroyd, H. et al. (2015). SOD1 protein aggregates stimulate macropinocytosis in neurons to facilitate their propagation. *Mol. Neurodegener* **10**, 57. doi:10.1186/s13024-015-0053-4

Zeineddine, R., Farrawell, N. E., Lambert-Smith, I. A. and Yerbury, J. J. (2017). Addition of exogenous SOD1 aggregates causes TDP-43 mislocalisation and aggregation. *Cell Stress Chaperones* **22**, 893-902. doi:10.1007/s12192-017-0804-y

Zhu, C., Beck, M. V., Griffith, J. D., Deshmukh, M. and Dokholyan, N. V. (2018). Large SOD1 aggregates, unlike trimeric SOD1, do not impact cell viability in a model of amyotrophic lateral sclerosis. *Proc. Natl. Acad. Sci. USA* **115**, 4661-4665. doi:10.1073/pnas.1800187115

Ziȩtkiewicz, S., Lewandowska, A., Stocki, P. and Liberek, K. (2006). Hsp70 Chaperone machine remodels protein aggregates at the initial step of Hsp70-Hsp100-dependent disaggregation. *J. Biol. Chem.* **281**, 7022-7029. doi:10.1074/jbc.M507893200

Table S1. Cell mask parameters for the analysis of relative fluorescence intensities of EGFP and mCherry using the IncuCyte Zoom basic analyser.

Cell-line	Fluorescent protein	Channel	Exposure (ms)	Background correction	Edge sensitivity	Data presentation
Neuro-2a	EGFP	Green	400	Top-hat (50 µm, 2 GCU)	-15	GCU × µm^2/ image
	mCherry	Red	800	Adaptive (2 RCU)	0	RCU × µm^2/ image

Table S2. Mask parameters for the analysis of relative fluorescence intensities of individual cells in confocal imaging experiments using Cell Profiler.

Object identified	Input image	Diameter (pixel units)	Threshold strategy	Thresholding method	Threshold boundaries	Distinguish clumps	Dividing lines in clumps
Nuclei	Hoechst	20-100	Automatic	-	-	Intensity	Shape
Cells	mCherry	20-65	Global	Otsu	0.01-1.0	Intensity	Propagate
	EGFP	-	Global	Otsu	0.0-1.0	-	-
Inclusions	Cerulean	15-40	Global	Otsu	0.01-1.0	Intensity	Shape

Table S3. Compensation matrix used to compensate samples co-expressing Cerulean and EGFP fluorescent proteins

|	[405] 450/50 nm	[488] 525/50 nm
[405] 450/50 nm	100 %	0.17 %
[488] 525/50 nm	1.4 %	100 %

pminHsp70p-EGFP plasmid map:
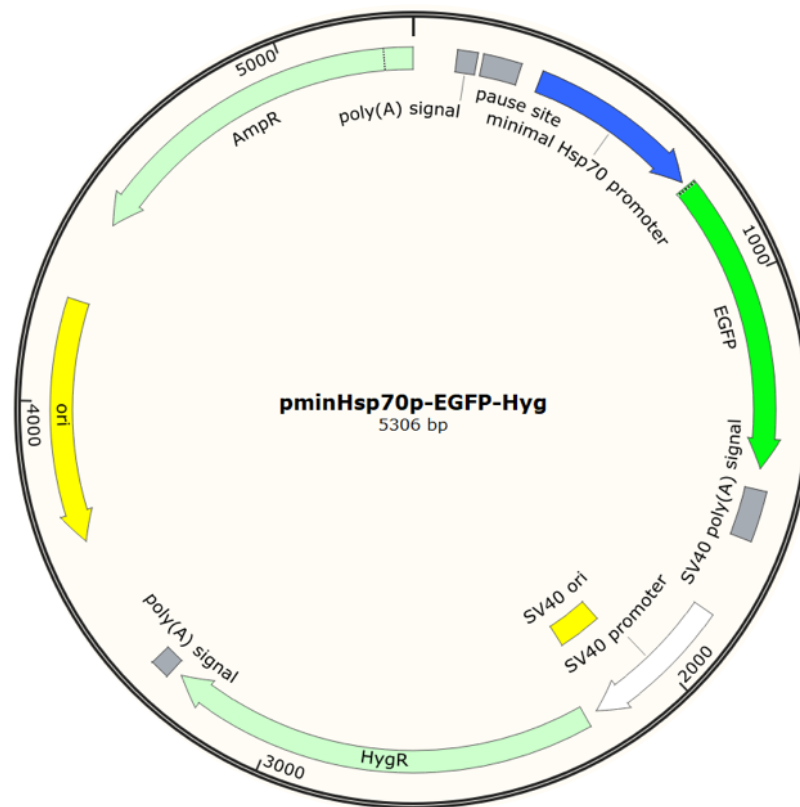
pminHsp70p-EGFP sequence:

TCGAGGCGCGTCCTCAGAGCCAGCCGGGAGGAGCTAGAACCTTCCCCGCGTTTCTTTCAGCAGCCCTG
AGTCAGAGGCGGGCTGGCCTGGCATAGCCGCCCAGCCTCTCGGCTCACGGCCCGATCCGCCCGAACCT
TCTCCCGGGGTCAGCGCCGCGCTGCGCCGCCCGGCTGACTCAGCCCGGGCGGGCGGGCGGGAGGCTCT
CGACTGGGCGGGAAGGTGCGGGAAGGTTCGCGGCGGCGGGGTCGGGGAGGTGCAAAAGGATGAAAAGC
CCGTGGAAGCGGAGCTGAGCAGATCCGAGCCGGGCTGGCGGCAGAGAAACCGCAGGGAGAGCCTCACT
GCTGAGCGCCCCTCGACGGCGGAGCGGCAGCAGCCTCCGTGGCCTCCAGCATCCGACAAGAAGCTCTC
TAGTCGACGGTATCGATAAGCTTCTTAACATATGGTGAGCAAGGGCGAGGAGCTGTTCACCGGGGTGG
TGCCCATCCTGGTCGAGCTGGACGGCGACGTAAACGGCCACAAGTTCAGCGTGTCCGGCGAGGGCGAG
GGCGATGCCACCTACGGCAAGCTGACCCTGAAGTTCATCTGCACCACCGGCAAGCTGCCCGTGCCCTG
GCCCACCCTCGTGACCACCCTGACCTACGGCGTGCAGTGCTTCAGCCGCTACCCCGACCACATGAAGC
AGCACGACTTCTTCAAGTCCGCCATGCCCGAAGGCTACGTCCAGGAGCGCACCATCTTCTTCAAGGAC
GACGGCAACTACAAGACCCGCGCCGAGGTGAAGTTCGAGGGCGACACCCTGGTGAACCGCATCGAGCT
GAAGGGCATCGACTTCAAGGAGGACGGCAACATCCTGGGGCACAAGCTGGAGTACAACTACAACAGCC
ACAACGTCTATATCATGGCCGACAAGCAGAAGAACGGCATCAAGGTGAACTTCAAGATCCGCCACAAC
ATCGAGGACGGCAGCGTGCAGCTCGCCGACCACTACCAGCAGAACACCCCCATCGGCGACGGCCCCGT
GCTGCTGCCCGACAACCACTACCTGAGCACCCAGTCCGCCCTGAGCAAAGACCCCAACGAGAAGCGCG
ATCACATGGTCCTGCTGGAGTTCGTGACCGCCGCCGGGATCACTCTCGGCATGGACGAGCTGTACAAG
TAA

Figure S 1. Plasmid map and sequence of the pminHsp70-EGFP-Hygʳ construct used to generate the Neuro-2a (HSE:EGFP) and HEK293 (HSE:EGFP) stable cell line reporters of the HSR. Sequence corresponding to the human minimal Hsp70 promoter (minHsp70p) is shown in blue and the EGFP gene in green. The 8 putative heat shock elements (NGAAN) in the minHsp70p sequence are underlined.
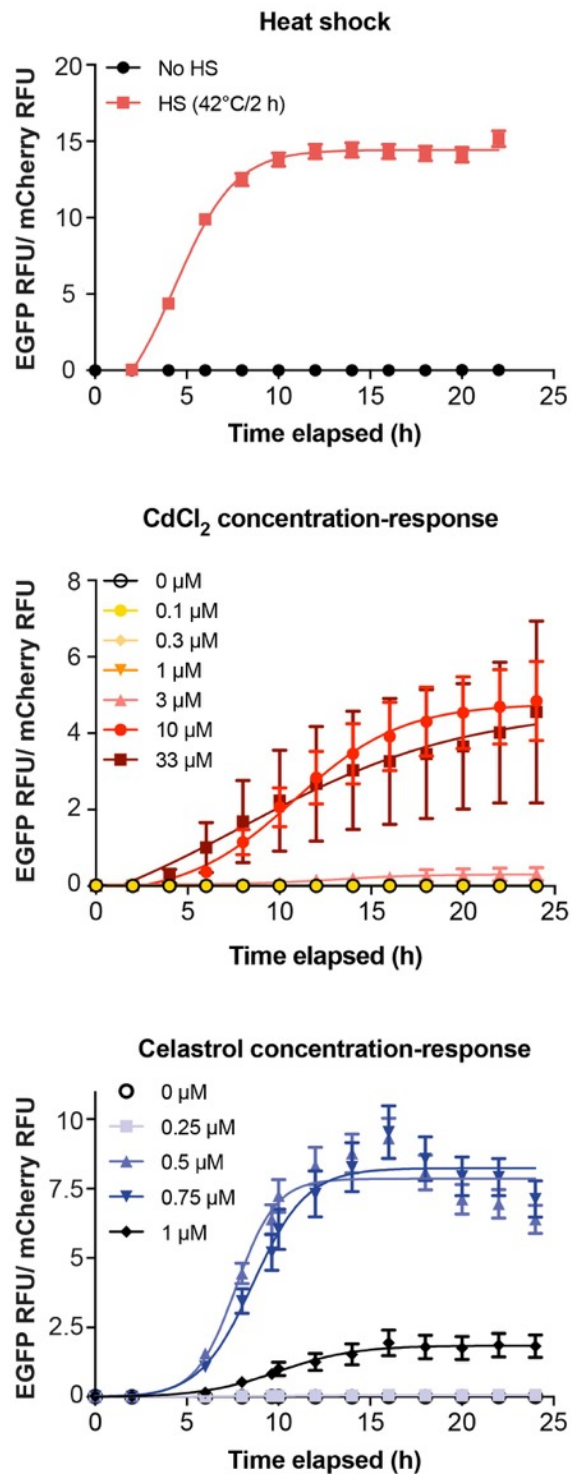
Figure S2. Monitoring induction of the heat shock response in Neuro-2a (HSE:EGFP) cells following heat shock, or treatment with CdCl$_2$ or celastrol . Cells were subjected to heat shock (42 °C/ 2 h), or log and ½ log doses of CdCl$_2$ (0-33 μM) or celastrol (0-1 μM). Following treatment cells were imaged every 2 h using an IncuCyte Live Cell Imaging System to monitor the levels of EGFP as a measure of HSR induction. Data is presented as the fold change in EGFP RFU over time, normalised to mCherry RFU, to account for changes in cell density over the time-course of the experiment. The data shown is the mean ± SEM of three independent repeats.
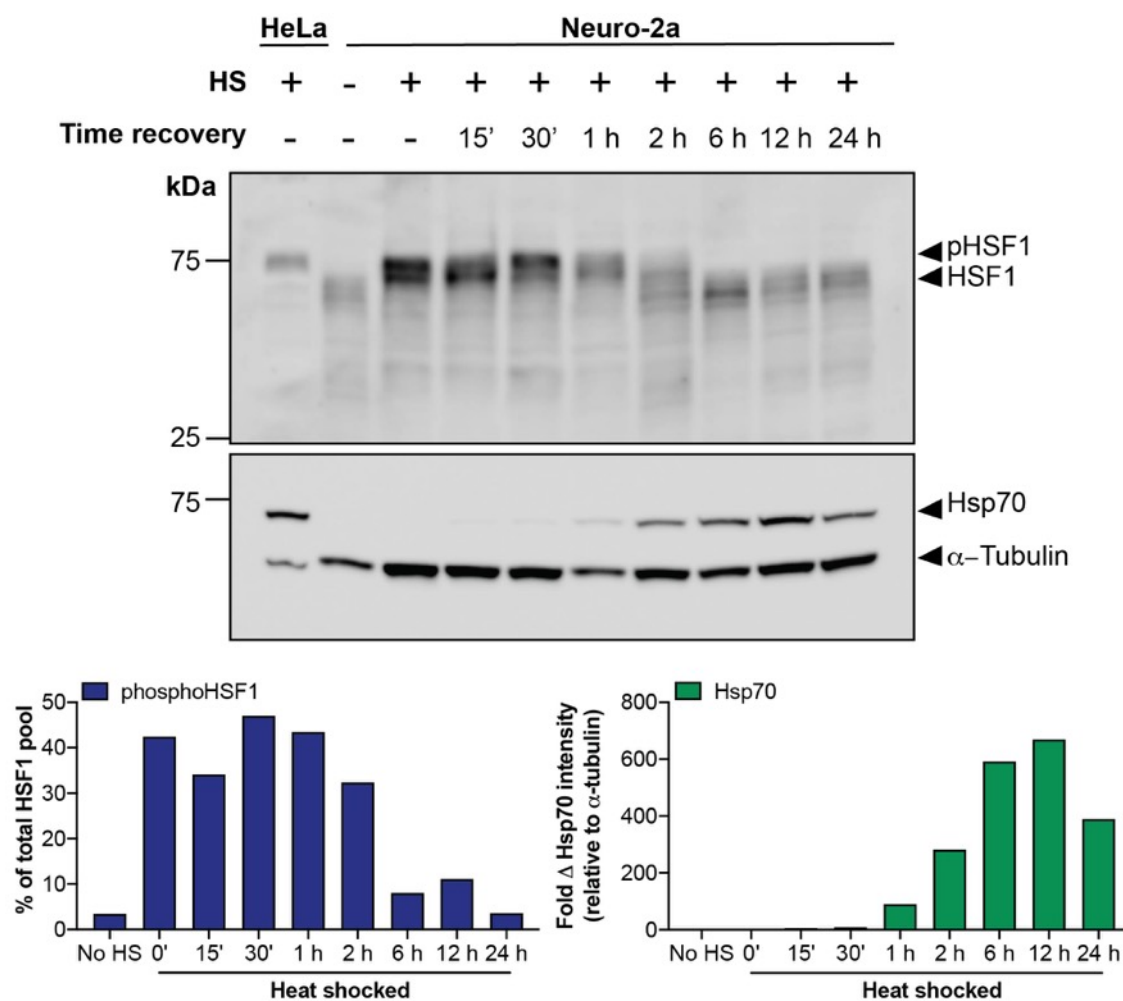
Figure S3. The HSR is induced in Neuro-2a cells after heat shock at 42°C for 2 h.
Parental Neuro-2a cells were heat shocked (HS) at 42 °C for 2 h and allowed to recover at 37°C for different time intervals (0,15 and 30 min, and 1, 2, 6, 12, and 24 h). For each time interval, whole cell lysates were prepared for immunoblotting and probed for markers of HSR induction. The HSR markers used were HSF1 activation (phosphorylation; pHSF1, 75 kDa, and HSF1, 70 kDa), and Hsp70 (70 kDa) up-regulation, α-tubulin (50 kDa) as a housekeeping protein to determine relative protein loading. HeLa cells heat shocked at 42°C for 2 h with no recovery were used as a positive control sample for each of the markers of HSR induction. Immunoblot analysis and densitometry showed that HSF1 was activated under these heat shock conditions and displayed hyper-phosphorylated bands after heat shock that persisted for up to 2 h post-heat shock. After 6 h of recovery at 37 °C the phosphorylation status of HSF1 had returned to control (no heat shock) levels. There was a time-dependent increase in Hsp70 levels, such that it was first detected 15 min after heat shock and reached a maximum after 6-12 h. Data shown are from one independent repeat.
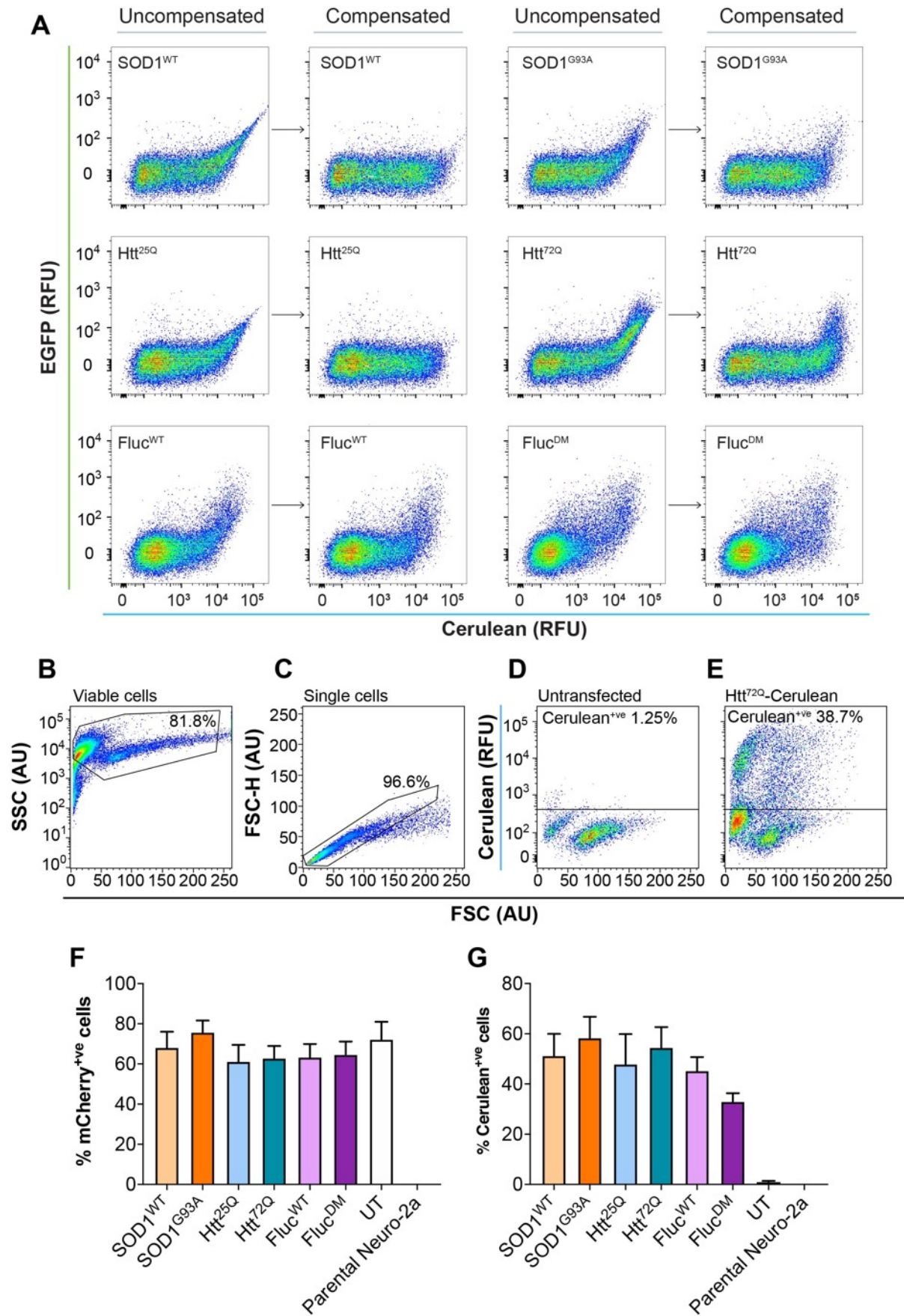
Figure S4. Flow cytometric data from Neuro-2a (HSE:EGFP) expressing EGFP and Cerulean fluorescent proteins were compensated to account for spectral overlap prior to analysis of HSR induction. Neuro-2a cells were transfected to express cerulean tagged SOD1^{WT}, SOD1^{G93A}, Htt^{25Q}, Htt^{72Q}, Fluc^{WT}, or Fluc^{DM} proteins and, 48 h post-transfection, cells were analysed by flow cytometry. (A) Due to the spectral overlap between Cerulean and EGFP fluorescence emissions it was necessary to compensate the flow cytometric data. Bivariate plots of EGFP and Cerulean fluorescence are shown for each of the samples before ("uncompensated") and after ("compensated") spectral compensation. Representative cytograms presented here are the same as in Figure 3 in the main text. (B) Plots of FSC and SSC of cells were used to resolve cellular debris and cell clumps. A polygonal gate was set around cells of interest and all downstream analyses was performed on this population. (C) Plots of FSC-height (FSC-H) and FSC-area (FSC-A) were used to resolve singlet and doublet events and a polygonal gate was used to exclude all doublets from downstream analyses. (D) Untransfected cells were used as a cerulean^{-ve} control to identify Cerulean^{+ve} events. (E) Representative plot of Neuro-2a (HSE:EGFP) cells transfected to express Htt^{72Q}-cerulean are shown and the percent of Cerulean^{+ve} cells in the gate are denoted. Data shown are representative of three independent repeats. (F) The proportion of cells that were mCherry positive in each sample. (G) The transfection efficiency, determined by the proportion of Cerulean^{+ve} cells, in each sample.
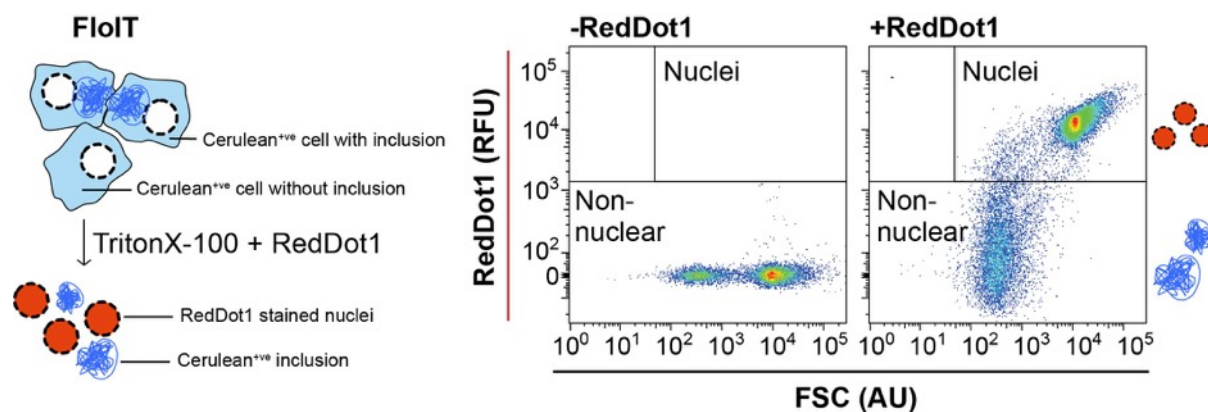
Figure S5. Flow cytometric analysis of inclusions and trafficking (FloIT) was used to determine the relative propensity of each protein to form inclusions in cells. Transfected cells were lysed with 0.1% TritonX-100 supplemented with RedDot1 nuclear stain and analysis by flow cytometry. Cells were first lysed in the absence of RedDot1 to set square gates to capture RedDot1[+ve] events and RedDot[-ve] non-nuclear events. Plots of forward scatter (FSC; size) and RedDot1 nuclear dye fluorescence used to enumerate the nuclei in the cell lysates.
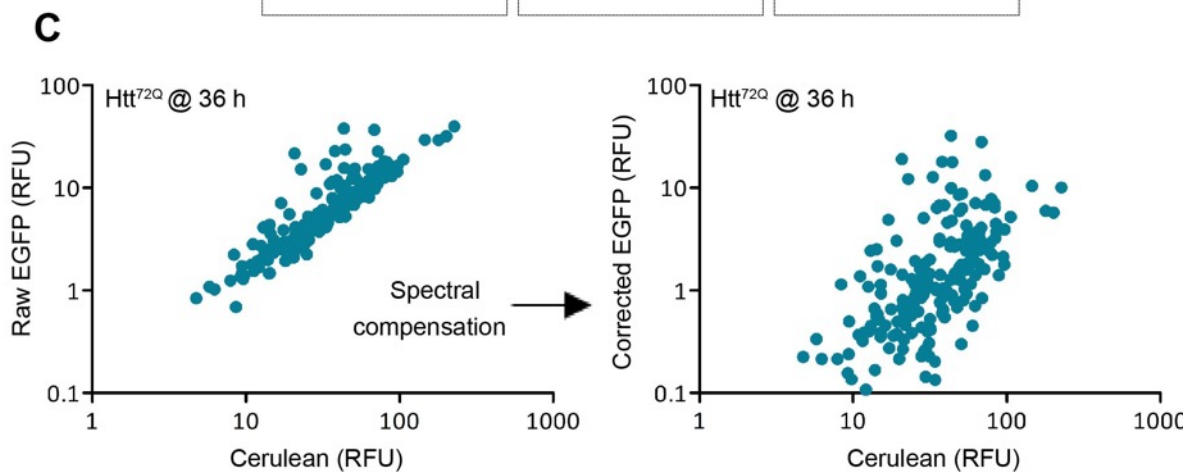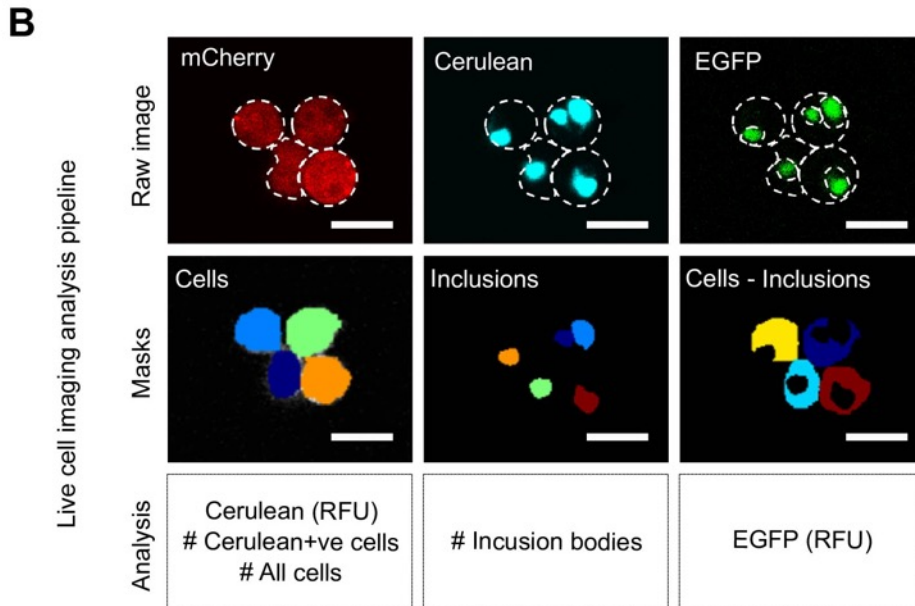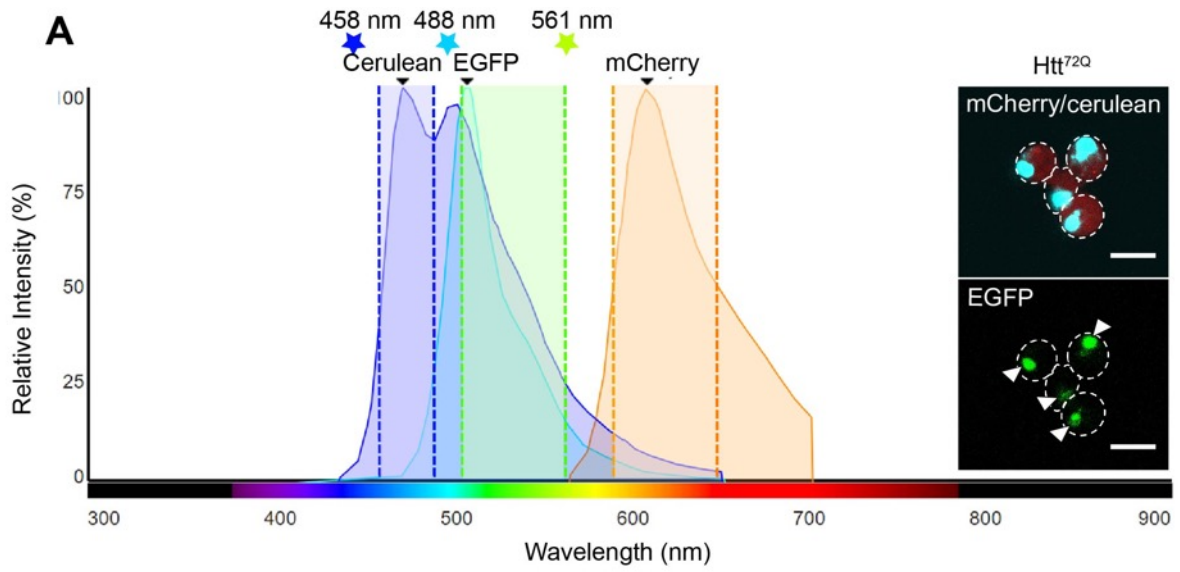
$$Raw\ EGFP - \left(\frac{Raw\ Cerulean}{1} \times \frac{13}{100}\right) = Corrected\ EGFP$$

Figure F6. Experimental design and analysis of live cell imaging experiments. Neuro-2a (HSE:EGFP) cells were transfected to express Htt[72Q] or Fluc[DM] and imaged over time by confocal microscopy. (A) Fluorescence emission spectra of cerulean, EGFP and mCherry fluorescent proteins. The windows for emission collection were set at 462-492 nm (blue dotted lines), 506-563 nm (green dotted lines), and 600-657 nm (orange dotted lines), for cerulean, EGFP and mCherry, respectively. The lasers used to excite each fluorescent protein are depicted by the coloured stars. Inset: A representative image of Neuro-2a (HSE:EGFP) cells transfected to express Htt[72Q], demonstrating spectral overlap between the cerulean and EGFP channels (white arrowheads). (B) Analysis pipeline used in Cell Profiler of confocal images acquired during the live cell imaging experiment. The mCherry channel (*left*) was used to define the "cells", which are masked in different colours, and this region was used to measure Cerulean fluorescence intensity, the number of Cerulean[+ve] cells, and the total number of all cells in each image over the time-course. The cerulean channel (*middle*) was used to identify "inclusions" and this region was used to count the number of inclusions formed in each image over the time-course. The "inclusions" were subtracted from the "cells" to generate a third region for measurement defined as "cells – inclusions", and this region was used to determine the EGFP fluorescence intensity in this channel. All scale bars = 20 µm. (C) Bivariate plots of cerulean and EGFP fluorescence intensities from the "cell – inclusions" region in Htt[72Q] transfected cells at 36 h, before (left) and after (right) spectral compensation. (D) Equation used to apply spectral compensation on the EGFP data.